

BBC RD 1979/6



RESEARCH DEPARTMENT



REPORT

**DIGITAL RECORDING USING
HOLOGRAM ARRAYS:
laser-beam deflection
and modulation**

K. Hacking, B.Sc.
I. Childs, B.A., Ph.D.

**DIGITAL RECORDING USING HOLOGRAM ARRAYS:
LASER-BEAM DEFLECTION AND MODULATION**

**K. Hacking, B.Sc.
I. Childs, B.A., Ph.D.**

Summary

The feasibility of optical methods of recording a digital television signal in real-time depends inter-alia on the successful development of devices for modulating and deflecting laser beams. For recording using the holographic approach, these devices must be able to handle many data channels in parallel and be optically efficient. Various methods have been investigated, and the more promising solutions are examined here in more detail. It is concluded that a solid-state digital light deflector together with a PLZT page composer could, with some further development, meet the basic recording requirements for digital television signals. For replay, an acousto-optic deflector of modest resolving power is eminently suitable.

Issued under the authority of



**Research Department, Engineering Division,
BRITISH BROADCASTING CORPORATION**

Head of Research Department

March 1979

(PH-166)

DIGITAL RECORDING USING HOLOGRAM ARRAYS: LASER-BEAM DEFLECTION AND MODULATION

Section	Title	Page
	Summary	Title Page
	List of symbols	1
1.	Introduction	1
2.	System objectives	1
3.	Light-beam deflection	4
3.1.	General considerations	4
3.1.1.	Recording	4
3.1.2.	Replay	5
3.2.	Principles of non-mechanical deflectors	5
3.2.1.	Acousto-optic methods	5
3.2.2.	Electro-optic methods	8
3.3.	The digital light deflector	8
3.3.1.	General characteristics	9
3.3.2.	Polarisation switches	12
3.3.2.1.	Optical switching efficiency	15
3.3.2.2.	Piezo-electric effects	15
3.3.2.3.	Electroding	19
3.3.2.4.	Thermal effects	21
3.3.3.	High-voltage switches	21
4.	Hologram page composers	21
4.1.	General considerations	21
4.2.	Electro-optic materials	22
4.3.	Characteristics of PLZT	23
4.4.	Design of electrodes	24
4.5.	Switching performance of PLZT	26
4.6.	Multipoint configurations	31
4.7.	Suitability of PLZT for use in a holographic recorder	33
5.	Conclusions	33
6.	References	33
	Appendix: Description of 2 kV switch circuit	35

DIGITAL RECORDING USING HOLOGRAM ARRAYS: LASER-BEAM DEFLECTION AND MODULATION

K. Hacking, B.Sc.

I. Childs, B.A., Ph.D.

List of symbols

M	= no. of modulator beams
τ_1	= exposure interval (dwell time)
τ_2	= access time in deflector
f^2	= focal length
p	= spatial frequency (cycles/mm)
v	= relative velocity
v_m	= velocity of acoustic waves
k_j	= coefficients ($j = 1, 2$, etc.)
θ	= angle of incidence
ψ	= 1st order diffraction angle
d	= width of deflector aperture
λ	= optical wavelength
h	= hologram spot diameter (effective)
B	= bandwidth (Hz)
l	= crystal length
l_s	= scan length
l_p	= prism spacing
α	= angular range of deflector
ω_s	= angular velocity of scan
n, n_o, n_e	= refractive indices
a, b	= coefficients
N	= no. of stages in digital light deflector
V	= voltage
V_π	= half-wave voltage
S	= switching rate (transitions/sec.)
β_j	= angular separation produced by Wollaston prism in j th stage
A_j	= Wollaston prism angle in j th stage
w	= separation of electroded faces
X, Y, Z	= crystal axes
ϕ	= phase retardation
E	= electric field (Volts/metre)
R	= no. of resolvable spots
g	= fraction of incident light not switched
I	= light intensity
D	= dielectric charge field
P_{ac}	= acoustic-wave power
r_{63}	= electro-optic coefficient
η	= strain contribution to electro-optic coefficient
ω	= angular frequency (radians/sec.)
Q	= ratio of stored to lost energy per half cycle

1. Introduction

The potentialities of digital recording systems based on optical methods are such that an increase in packing density (bits/unit area) of nearly two orders of magnitude is possible, as compared with that so far achieved with magnetic recording techniques. The impetus for these optical developments has come from the growing need for computer data banks of large capacity providing rapid access to blocks of information. A comprehensive review of the state-of-the-art in optical methods of data storage has recently been published by Chen and Zook.¹

The possibility of constructing an optical recorder for the storage of digital television signals in real-time was investigated prior to 1970.² Later, the possible application of holographic techniques to construct a digital television recorder was envisaged, making use of the highly coherent properties of a laser beam.³ However, it was clear that the sophisticated optical devices required to exploit the holographic concept fully, at the high information transfer rate associated with digital television signals, were yet to be developed. It was necessary to think initially in terms of compromise arrangements, such as serially recording relatively small holograms⁴ arranged in suitable patterns. The general characteristics and feasibility of recording such micro-hologram arrays on photographic film were assessed and formed the subject of a previous report.⁵

Work has continued with the aim of setting-up an experimental real-time digital recording and replay system, in order to evaluate further the potential of the holographic approach. Two optical devices, which are crucial to the success of the project, are a hologram page-composer and a laser-beam deflector, both capable of handling up to fifty independent beams of light simultaneously. The purpose of this report is to present the characteristics of selected methods of modulation and of deflection which, it is believed, can provide a feasible solution to the problem. From this study and from experimental measurements on samples of suitable materials, it is suggested how devices could be constructed which would form the basis of an experimental system with relatively modest performance objectives.

2. System objectives

Before discussing page composers and deflectors, it seems appropriate to outline a possible recording system and prescribe some performance objectives. This will give some indication of the task required of the devices to be discussed in this report. One such arrangement is shown in Fig. 1; where the principal components of the record process (Fig. 1(a)) and the replay process (Fig. 1(b)) are presented schematically. The general format structure of the recorded hologram array envisaged is shown in Fig. 1(c).

In the record process, the output beam of a continuous wave laser is formed into an array of parallel beams that are then directed through a multiport modulator arrangement. Each beam can be considered as a 'digit' beam, and the purpose of the modulator is to switch the state of the digit beams (i.e. 'on' or 'off') in accord with incoming binary data;* if there are M beams, then M switching ports are

* The incoming data (assumed serial) would be demultiplexed, assembled in small buffer stores, and the modulator ports set simultaneously at clocked intervals.

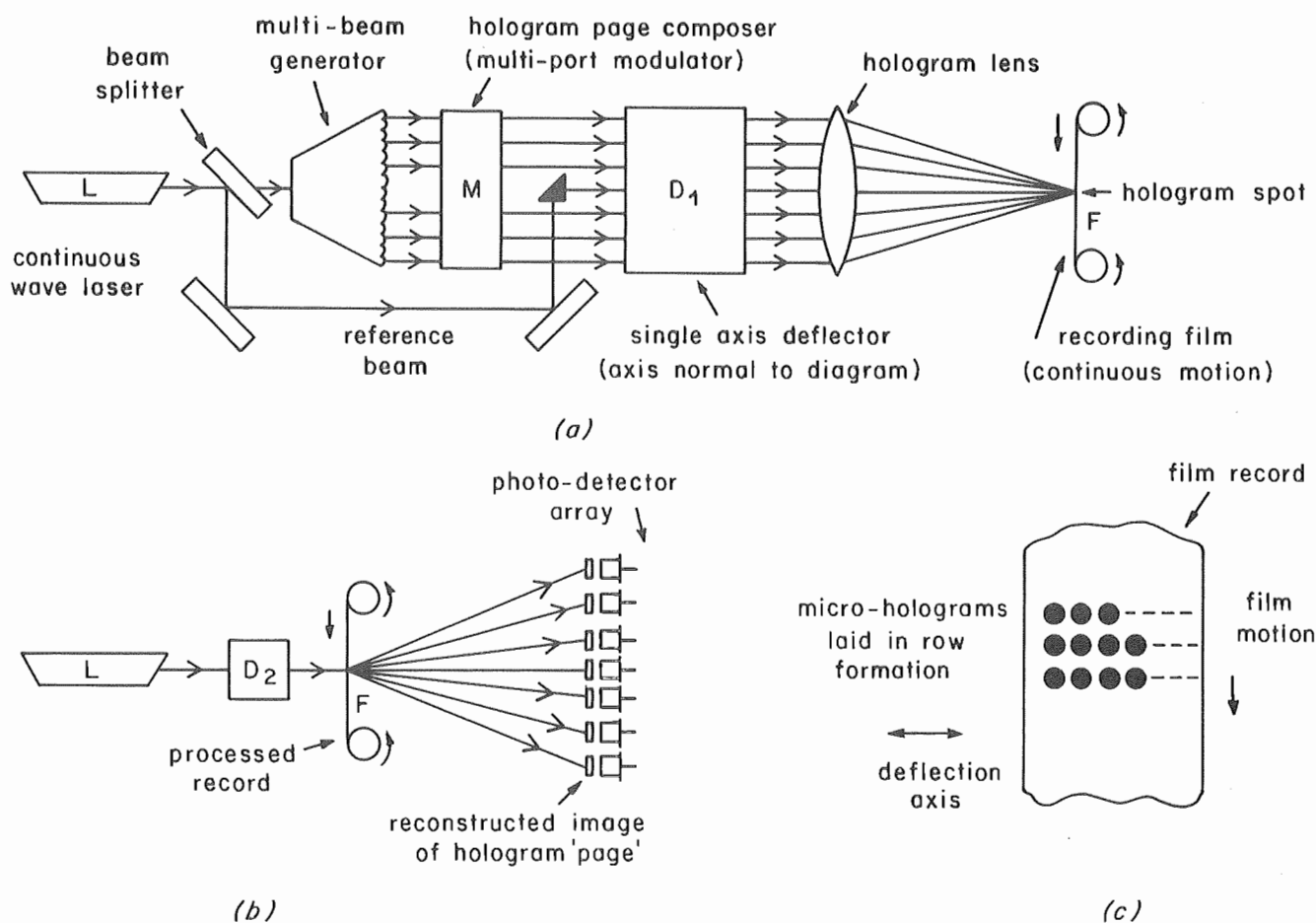


Fig. 1 - Basic system arrangement

(a) Record process (b) Replay process (c) Recorded hologram format

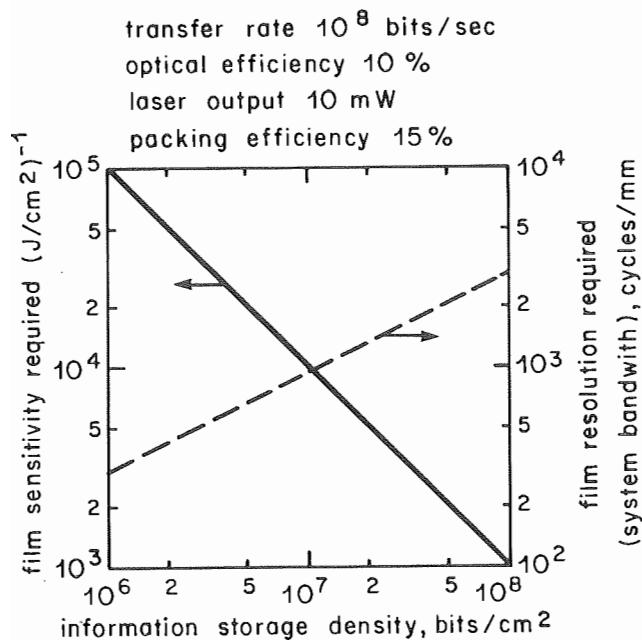
required in the modulator (or M modulators) each independently addressed. The array of beams emerging from the modulator at any one instant corresponds to one 'page' of the incoming digital data. This multiport device is known as the hologram page-composer or simply the page composer. A stronger reference beam is then combined with the parallel array of beams emerging from the page composer and the whole passed through a deflector before being brought to a focus by a lens on to the recording medium. The focused spot exposes the recording medium and forms a micro-hologram of the composed 'page' of information. Before the exposure of the next hologram (containing the next 'page' of data to be recorded) the deflection angle for the array of beams is changed so that the focused spot is directed to the next site. Although various formats are possible, it is convenient to think of a straightforward sequential exposure of individual holograms with centres on a line running across the film, i.e. approximately orthogonal to the film motion. The recording of the next line of holograms is begun when the deflection has completed one scan cycle, during which time the film has advanced by an appropriate distance to avoid the holograms overlapping with those of the previous line.

In the replay process, a laser beam passes through a deflector and is focused on the film such that the spot is

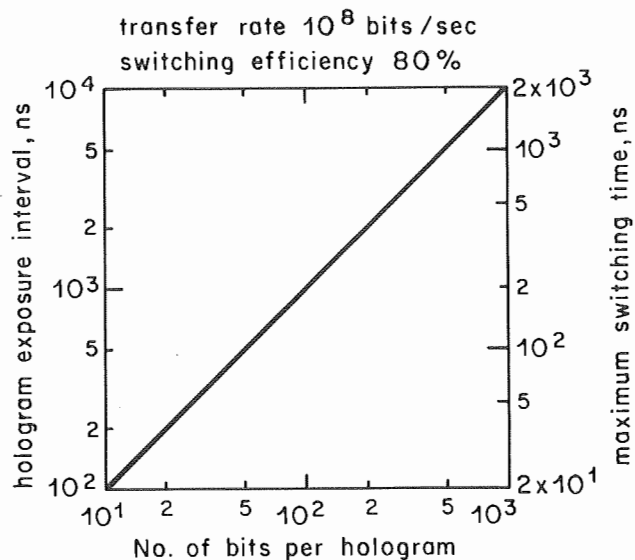
about the same size as the recorded holograms and is synchronised so that each line of holograms is consecutively scanned. The reconstructed image of the original page of data appears, on the far side of the film (assuming transmission holograms), as the interrogating beam passes over a hologram. An array of photodetectors, relatively spaced to correspond with the geometrical pattern of the original page, is placed so as to intercept the reconstructed image. The output of a given detector should then correspond precisely with the original input data fed to that particular position in the page.

From previous experiments, and an analysis of available information, it was estimated that components could be developed which would permit a recording and replay experiment to be set up with the following basic specification:—

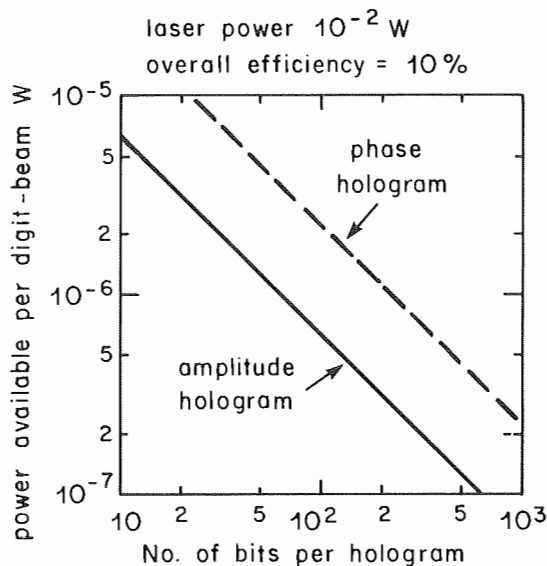
1. A reel-to-reel system using unperforated 8 mm or 16 mm high-resolution film.
2. Continuous motion of the film past the recording and replay stages at a speed less than 1 metre/sec.
3. No moving parts except for the continuous film transport.



(a)



(b)



(c)

Fig. 2 - Basic system parameters

- (a) Record process: film requirements as a function of storage density
(b) Record process: exposure interval and maximum switching time as a function of number of bits per hologram
(c) Replay process: reconstructed image power as a function of number of bits per hologram

4. An average information storage density greater than 10^6 bits/cm².
5. An information transfer rate of 10^8 bits/sec. in both the recording and replay modes.
6. Laser radiation powers less than 10^{-2} Watts.
7. Recording system aperture $f/2.8$ (f = focal length).
8. Reconstruction signal-to-noise ratios better than 20 dB.

Figure 2 illustrates the typical relationships which exist between some of the system parameters. In Fig. 2(a) the film sensitivity* and resolution required are shown as a function of storage density, assuming the particular conditions stated in the Figure.

* For amplitude holograms using photographic film, the sensitivity required is that which will give an optical density of 0.6 above base with appropriate development, after making allowance for any reciprocity failure due to short exposure times ($\approx 10^{-6}$ secs.).

The period available for hologram exposure and the maximum switching times available for both the page composer and the deflector stages are, for a given transfer rate, directly proportional to the number of bits per hologram; this is shown in Fig. 2(b). If it is assumed that a continuous-wave laser system is used and that the maximum available intensity is maintained for 80% of the hologram exposure interval, then the maximum switching times (rise and fall times) required are indicated by the R.H. scale in Fig. 2(b).

Fig. 2(c) refers to the replay process and shows, for both amplitude-type holograms and phase-type holograms, the optical radiation power available (for the 'on' state) in each digit-beam of the reconstructed image, as a function of the number of bits per hologram; the plots assume a laser primary output power of 10^{-2} W and a system efficiency of 10% (to allow for losses in the scanning arrangement and non-linear effects in the recording medium).

The spot holograms referred to in this report are assumed to be two-dimensional and of the 'on-axis' or 'base-band' type⁵ (making use of spectral interleaving to avoid crosstalk when simultaneously exposed) as opposed to the more usual 'off-axis' or 'carrier' type. The latter type requires at least twice the system bandwidth* than the former, for a given data storage density.

The advantages of the holographic concept are best exploited by using holograms with the largest possible area but, if constant storage density is to be maintained, this means increasing the number of bits per recorded hologram; as will be seen from Fig. 2(b), this has also the advantage of relaxing the switching requirements of the page-composer and deflector stages. On the other hand, the page-composer then requires a larger number of switching ports, each capable of bring independently but simultaneously driven. Moreover, in the replay process, the optical power available for the photodetection of each reconstructed digit-beam varies inversely with the number of bits per hologram. This would not matter if the only 'noise' appearing at the output of each detector in the array were due to photon noise in the digit beam and/or 'shot' noise in the detector, because this problem could be overcome by increasing the incident laser power. Unfortunately a large contribution to the 'noise' at a detector output is expected to arise from the background scatter of laser light due to the granularity and surface defects of the recording medium, and these scatter levels increase directly with the incident power of the reconstruction laser-beam; thus the noise level tends to increase with the output signal.

Previous experiments using amplitude-type micro-holograms, recorded on holographic film, have indicated that at storage densities of about 10^6 bits/cm² it would be feasible to use up to 50 bits per hologram and still maintain a signal-to-background-noise ratio adequate for decoding

with low error rates. Larger capacity holograms, perhaps containing several hundred bits, are believed to be feasible with thin phase-type holograms.

It may be seen from Fig. 2(b) that, for 50-bit holograms, the maximum switching times required of the ports in the page composer and of the deflector stages are of the order of 100 ns, with holograms exposure intervals of 500 ns, i.e. at a maximum switching rate of 2×10^6 transitions per second.

In order to achieve an average storage density of 10^6 bits/cm², the area occupied by a 50-bit hologram cannot be greater than about 5×10^{-5} cm² which, assuming holograms of circular form, corresponds to a hologram diameter of about 60 microns. Further, assuming 60 microns also to be the minimum spacing between the holograms in the recorded array, it is necessary to write at least 120 holograms across the film in order to keep the film transport velocity below 1m/sec. Thus the deflectors for recording and replay need to be single-axis types with resolutions of at least 120 spots, and with effective transverse scan velocities of 2 spots per microsecond. Various modifications are possible by choosing elliptical shapes for the hologram spot, or even one-dimensional holograms. These arrangements amount to making greater demands with respect to the maximum spatial frequency (system bandwidth), required in one direction and less in an orthogonal direction. Although practical limitations may favour the adoption of some asymmetrical arrangements, it is apparent that the symmetrical two-dimensional hologram affords the greatest packing density for a given maximum film resolution or system bandwidth.

3. Light-beam deflection

3.1. General considerations

3.1.1. Recording

There are three basic approaches to the problem of deflecting laser beams in a regular scanning mode in order to record a line of holograms. One method is to produce a continuous angular deflection of the beams, e.g. by a rotating mirror, and to operate an exposing shutter at regular intervals to obtain a succession of hologram exposures. The second is to cause the hologram spot to dwell at one location for most of the exposure interval and then jump rapidly to an adjacent site; no exposing shutter is necessary if the ratio of dwell time to jump time is sufficiently great. The third method is similar to the second in that the spot dwells at each location, but the beam intensity fades rapidly at one location and simultaneously increases at an adjacent site. Thus, in this latter method, there is no relative motion whatsoever between the spot and the recording medium along the deflection axis. It should be noted that, for a continuous film-transport system, there is always relative movement of the hologram exposing radiation with respect to the film in the direction of the film motion. The movement in this direction, however, is very slow compared to that along the transverse deflection axis; for example, in the 50-bit system outlined in Section 2, the deflection-axis

* System bandwidth may be defined here as the maximum spatial frequency (cycles/mm) of any intensity (or phase) modulated component which represents wanted information within the hologram.

speed is 120 m/sec. compared with 1m/sec. approximately for the film transport.

Relative motion between the hologram exposing radiation and the recording medium can result in a blurring of some of the high-frequency interference structures in the recorded hologram, giving rise to a corresponding weakening of some of the reconstructed images. Let p_{\max} be the highest spatial frequency component of the hologram in the direction of a relative velocity ν between the exposing radiation and the recording medium. Then the relation between the permissible exposure time τ_1 and the spatial frequency is of the form

$$\tau_1 \leq k(p_{\max}\nu)^{-1} \quad (1)$$

where k is a coefficient depending on the reduction of modulation depth, due to blurring, which can be tolerated. For a constant radiation intensity during the exposure interval, it can be shown that the modulation depth is depressed by the factor $\text{sinc}(\pi k)$. Thus for $\text{sinc}(\pi k) = 0.9$, i.e. for a 10% reduction in modulation depth, $k = 0.25$ approximately. In the system under consideration, using 60 micron diameter 50-bit holograms, $p_{\max} \approx 300$ cycles/mm, $\nu = 0.94$ m/sec. in the film motion direction and $\nu = 120$ m/sec. along the deflection axis. Substituting these values in Equation (1), we find that the 'blurring' limits for the exposure interval in this case would be 880 ns for the film motion direction but only 7 ns for the transverse deflection. It is clear, therefore, that to use a continuous method of deflection with the exposing radiation moving at a uniform rate, pulsed operation of the laser source would be necessary, the pulses being less than 10 ns duration and having a repetition rate of 2 MHz.

The alternative deflection methods, which allow the exposing hologram radiation to dwell at each location, overcome the blurring problem in the direction of deflection. Moreover, if the hologram exposure interval is approximately 500 ns, there will be only a small reduction in modulation depth in the film-motion direction even without shuttering. This is convenient because a continuous-wave laser source can then be used efficiently.

Crosstalk between holograms in the recorded pattern is another problem that can be worsened by the limitations in the performance of the deflector. In continuous deflection systems, spatial overlapping of holograms can be caused by non-linearity of the scan and/or perturbations in the regularity of the exposure periods. In the other deflection methods, slow transitions between successive locations, or the inability to deflect all the exposing radiation to successive locations, can result in the contamination of a hologram site with information intended for neighbouring sites. The general effect of crosstalk will be to mar the quality of the reconstructed images and thus increase the probability of detection errors.

3.1.2. Replay

In the replay mode, a single unmodulated laser beam

* $\text{sinc}(\pi k) \equiv \sin(\pi k)/\pi k$.

is focused on the recording and then caused to scan each line of holograms in turn. Because of the properties of Fourier transform holograms, the quality of the reconstructed image is not affected by any movement of the interrogating reference beam across the hologram. Thus, in principle, any form of single-axis deflection having sufficiently good resolution could be used for replay.

The principal problem is to track the interrogating beam so that it scans over the hologram centres and keeps sufficiently well in register. It may be necessary for high-density recordings, using small-diameter holograms, to provide a closed-loop feedback arrangement in the replay system to maintain adequate tracking. This might well make use of an additional (low resolution) deflector, operating in the direction of film motion over a small angular range.

3.2. Principles of non-mechanical deflectors

Leaving aside rotating mirrors, and other well-known mechanical devices that have vibrating or moving components, there are two other types of deflector emerging as practical contenders for use with visible laser radiation. These are known as acousto-optic⁶ and electro-optic deflectors⁷ respectively. Several versions of these have been reviewed elsewhere.^{8,9}

3.2.1. Acousto-optic methods

In the acousto-optic type of deflector, an acoustic wave generated by a suitable ultrasonic transducer is propagated through a slab of glass or crystal, as indicated in Fig. 3(a). This compressional wave creates a periodic structure of varying refractive index within the medium; the index is greatest at the instantaneous peaks of the compressional wave and least at the troughs. A coherent light beam, traversing the slab almost at right angles to the acoustical wave, emerges from the medium with a systematic perturbation of phase over its wavefront in the direction of the acoustic wave. The maximum excursion of the phase perturbation is proportional to the length of the interaction path traversed and the variation of refractive index induced, the latter being a function of the acoustical power propagating through the medium. If the parameters are adjusted so that a phase excursion of 180° is created in the emerging wavefront, and the acoustical wavelength is small compared with the dimensions of the laser beam, then a grating-like diffraction effect is produced. The light energy is concentrated by this diffraction process at a number of angular directions, corresponding to the orders of the grating. These angular directions are in fact directly proportional to the frequency of the acoustic wave, and it is this linear relation which makes the principle so attractive for a deflector; thus scanning can be achieved by frequency modulating the acoustic wave.

To obtain an efficient practical device, use is made of the Bragg effect which occurs when there is a long interaction path and the beam is slightly inclined to the acoustic wavefront, as shown in Fig. 3(b). Calling the incident angle θ and the 1st order angles of diffraction $\pm\psi$, the Bragg angle condition occurs when $\theta = |\psi/2|$; the emerging light can

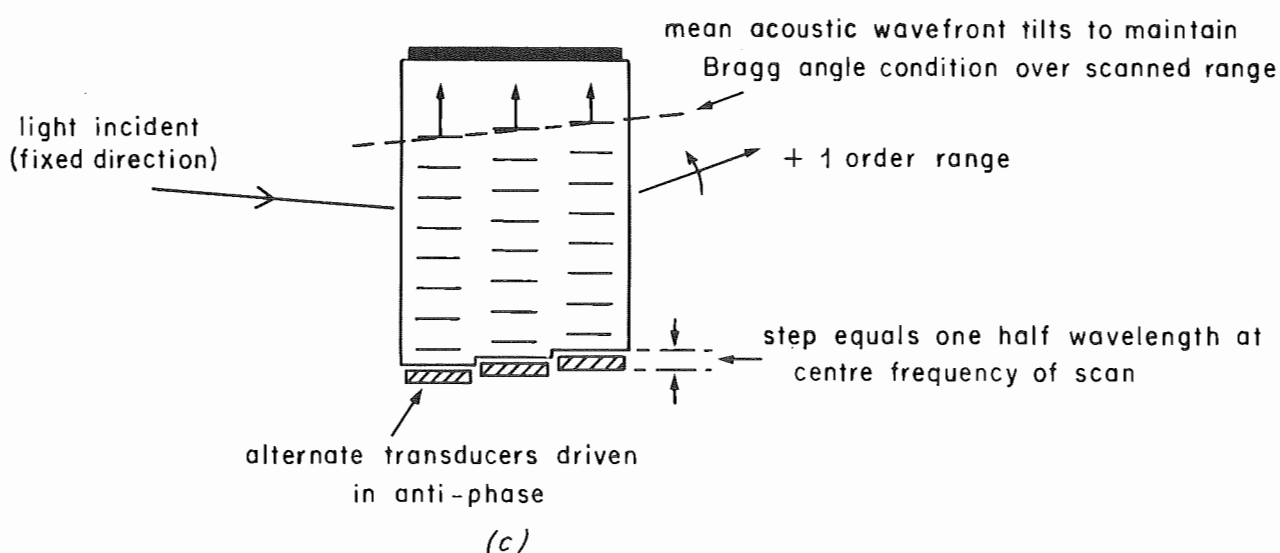
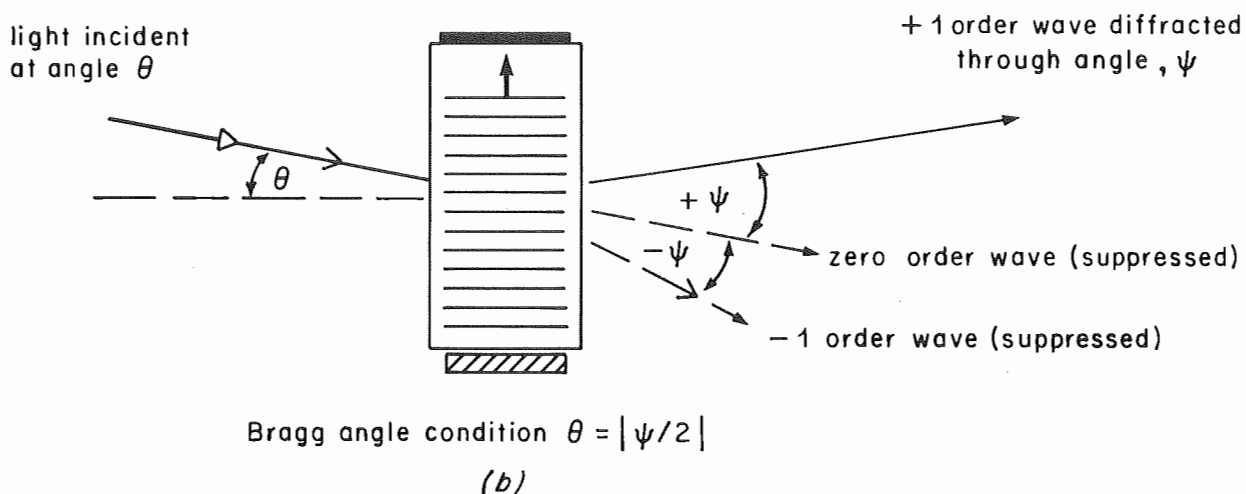
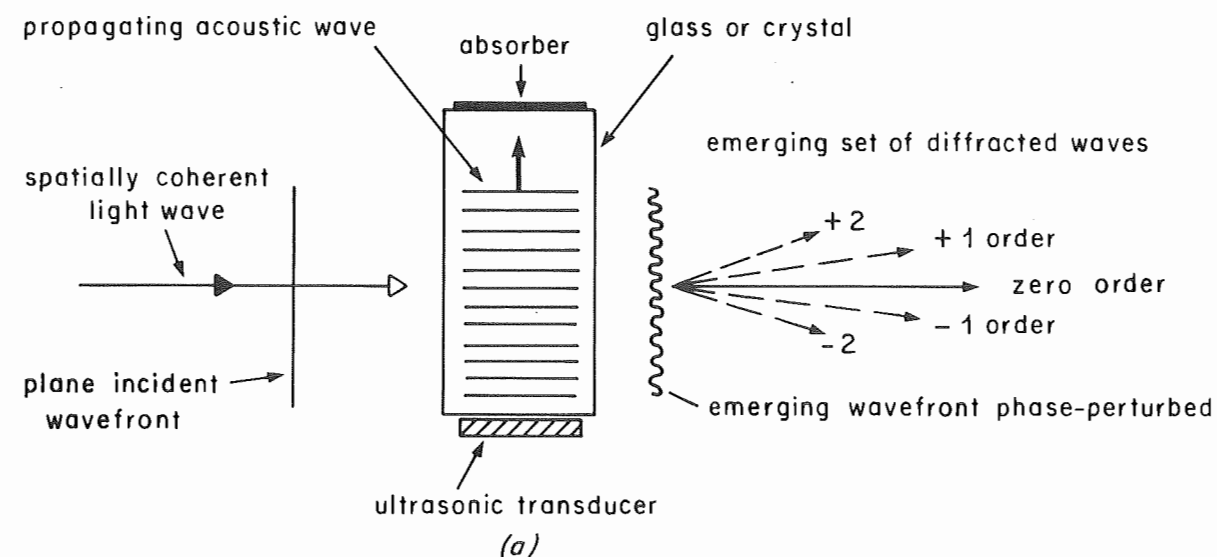


Fig. 3 - Acousto-optic deflection

(a) the basic interaction

(b) the ideal Bragg angle condition

(c) beam steering by stepped transducers

then be suppressed in all orders except the positive first order,* where it is in fact concentrated.

In a practical device the angle ψ of the emerging beam is varying with the frequency of the acoustical wave, and because the Bragg angle condition can only be precisely satisfied for one particular emergent angle ($\psi = 2\theta$) the optical efficiency would vary significantly over the deflection range. To avoid this limitation, Korpel¹⁰ proposed synthesising an acoustic wavefront in the medium which, in effect, progressively tilts towards the incident beam as the scanning frequency increases. This was achieved by using a number of ultrasonic transducers spread over the optical path length, as shown in Fig. 3(c). The individual transducers are physically stepped by one-half of the acoustic wavelength corresponding to the mid-frequency of the range necessary to provide the scan. Alternate transducers are driven in antiphase so that, at the mid-frequency, the acoustic wavefront is parallel to the transducer faces. At other frequencies, however, the mean acoustic wavefront is slightly tilted and helps to maintain the Bragg-angle condition.

Another limitation to the angular range of deflection is due to the acoustic absorption of the medium. This gives rise to a non-uniformity of acoustic power over the aperture (and hence non-uniform phase excursion). The effect limits the maximum frequency of the ultrasonic wave which can be used for a given aperture and medium.

One factor which determines the number of resolvable positions obtainable from the deflector is its effective aperture in the direction of scan. If the laser beam emerging from the deflector is brought to a focus with a perfect lens, then the diameter of the diffraction limited spot, h , is given by

$$h = k_1 f \lambda d^{-1} \quad (2)$$

where f = focal length of lens

λ = laser radiation wavelength

d = width of deflector aperture (in scanning plane)

The coefficient k_1 , depends on the aperture shape, the intensity distribution of the laser beam across the aperture, and on the criterion used to measure the spot size. For example, using the Rayleigh criterion associated with a uniform distribution of intensity over a circular aperture, $k_1 = 1.22$.

The angular range of the deflector, α , is set by the range of input frequencies, i.e. by the driver bandwidth, B . The relation is

$$\alpha \approx \lambda B v_m^{-1} \quad (3)$$

where v_m is the velocity of the acoustic wave in the medium.

* Because of the mirror symmetry of the emerging and incident beams with respect to the acoustic wavefront, this condition is often termed Bragg 'reflection' rather than 'diffraction'.

The number of spots, R , that can be resolved within the deflection range is $(f\alpha/h)$, which from Equations (2) and (3) can be expressed by

$$R \approx B d (k_1 v_m)^{-1} \quad (4(a))$$

It should be noticed from Equation (4(a)) that the number of resolvable spots is independent of the wavelength, λ , of the laser radiation. Another important parameter is the speed of response of the deflector, and this can be specified by the minimum time taken to deflect the spot from one position to any other in the scan. The minimum time taken to do this is equal to the time taken for an acoustic wavefront to cross the effective aperture (the latter may, in practice, be determined by the laser-beam diameter). Thus, the so called 'access time', τ_2 , of the deflector is equal to $d v_m^{-1}$, and substituting in Equation (4(a)) we obtain for the number of resolvable positions

$$R = B \tau_2 k_1^{-1} \quad (4(b))$$

Continuous regular scanning, line-by-line, is achieved by a linear increase, during the forward scan, in the input r.f. drive frequency with time;* during the fly-back period the initial frequency is re-established before the commencement of the next scan. It is clear that during the forward scan the travelling wave-structure within the interaction aperture has a linear frequency-gradation, ΔB , which is a function of the angular scan velocity ω_s and the effective width of the aperture d . The relationship is

$$\Delta B = \omega_s d \lambda^{-1} \quad (5)$$

At high scan-velocities, the frequency gradation significantly upsets the collimation of the emerging laser beam (in the direction of the acoustic wave propagation). Consequently, if a spherical lens of focal length, f , is used to focus the emerging beam under static conditions ($\Delta B = 0$) the focused spot will be elongated during the scan. If the application is such that the scan velocity can be kept constant, then this asymmetrical defocusing effect can be compensated by inserting a cylindrical lens of the correct power in the emerging beam. The focal length, f_c , required is

$$f_c = \pm v_m \omega_s^{-1} \quad (6)$$

The correct sign in Equation (6) depends on the relative directions of the acoustic wave propagation and the scan. Clearly, if cylindrical lens compensation is applied to the forward scan, spot elongation during the fly-back period will occur due to the reverse sign requirement as well as to the increased scan rate.

Lead molybdate (PbMoO_4), grown as a single crystal, is a useful medium with a high figure of merit for acoustic-optic deflectors. More recently, high-index glasses have been used; these are less expensive than crystals and generally have better optical quality. These materials can be

* The problems associated with wide-band r.f. drivers for an acoustic-optic cell, operating in the v.h.f. range, were examined by I. Childs in a previous Research Report.¹¹

used in the v.h.f. range of frequencies with bandwidths up to 150 MHz. By suitable matching and construction, devices with up to 10^3 spot resolution and with deflection efficiencies greater than 50% have been produced. The ultrasonic transducers are thin plates of either lithium niobate or PZT ceramic, and these are bonded to the side of the interaction medium (Fig. 3). Careful broad-band matching of the transducer impedance to the r.f. drive circuit is essential.¹¹

3.2.2. Electro-optic methods

Electro-optic deflectors are based on the small changes in refractive index which can be induced in various media by an applied electric field. In some materials a significant birefringence is induced and this forms the basis of a class of devices for controlling the polarisation characteristics of a light beam. In general, the electro-optic effect can be described by an equation of the form,

$$n = n_0 + aE + bE^2 + \dots \quad (7)$$

Where n is the refractive index, E is the applied electric field, a and b are coefficients depending on the medium, and n_0 is the refractive index with no field applied. In most transparent materials, the coefficients a and b are exceedingly small so that the electric field has to be correspondingly large to produce any significant effect. In a ferroelectric material the electro-optic effect usually becomes much stronger near the Curie temperature.

Equation (7) indicates the possibility of a linear effect when $a \gg b$, and a quadratic effect when $b \gg a$ or $a = 0$. The quadratic effect (known as the Kerr effect) occurs in liquids and some isotropic solids, where $a = 0$. The linear effect (or Pockells effect) is achieved in some anisotropic crystals where the coefficient a is dominant. Terms of higher order than the second can usually be neglected.

An example of the direct application of the electro-optic effect to produce a continuous or analogue deflector is shown in Fig. 4(a), where the deflection medium is a transparent crystal suitably cut in the form of a simple isosceles prism. Due to the linear (Pockells) effect, a voltage applied between electrodes on opposite sides of the prism alters the refractive index and hence the angle of emergence of a light beam (suitably polarised with respect to the field). It can be shown that maximum sensitivity occurs when the light beam travels parallel to the base within the crystal and that the number of resolvable positions is proportional to the base length of the prism. Electro-optic materials capable of being grown with good optical quality are required for constructing such prisms. The most popular of these are the tetragonal (42m point classification) crystals of potassium dihydrogen phosphate (KH_2PO_4) known as KDP, and the more sensitive deuterated version KD^*P . The sensitivity of these materials, however, only permits resolutions of several spots per centimetre of prism base length to be obtained. To increase the resolution it is necessary to cascade prisms in such a manner as to add the induced deflections while balancing out passive angular deviation.

An alternative approach is to combine a passive deflecting element with an electro-optic polarisation switch, as shown in Fig. 4(b). Here the actual beam deflection is carried-out by means of a uniaxial crystal, such as calcite, cut so that the emerging components are laterally displaced. Which path the light takes depends on the direction of polarisation of the beam incident on the crystal and this direction is controlled by the electro-optic polarisation switch. (Fig. 4(b).) The latter is a cell which rotates the plane of polarisation of a transmitted light beam through 90° when a certain voltage, V_π , is applied between two electrodes attached to the cell.

The basic pair of elements in Fig. 4(b) comprise one deflection stage which is essentially binary in operation, owing to the two alternative transmission paths available. A full deflector of this type, known as a digital light deflector, comprises N of these binary stages in tandem. The deflecting element in each stage is constructed to give twice the lateral deflection of that obtained in the preceding stage, as indicated in Fig. 4(c). Clearly, the total number of possible output positions is 2^N , and these can be arranged either as a rectangular array or as a line array. (A more detailed examination of the digital light deflector is given in Section 3.3).

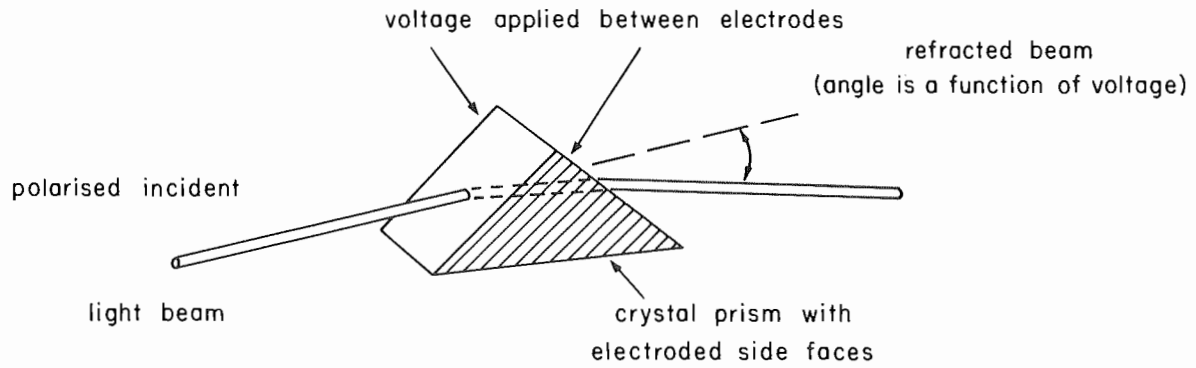
Either the quadratic (Kerr) effect or the linear (Pockells) effect can be used to operate the electro-optic polarisation switches, as only two fixed polarisation states are required in this application. With no voltage applied, an incident light beam which is plane polarised remains unchanged after passing through the cell. On application of a voltage V_π a birefringence is established in the cell such that a phase difference of π radians is introduced between the ordinary and extraordinary wave components. As a result, an incident light beam polarised at 45° to the induced birefringent axes has its polarisation rotated by 90° on emergence. (See Section 3.3.2).

The voltage V_π , known as the half-wave voltage, varies between a few hundred volts and tens of kilovolts depending on the material and the dimensions of the cell. If the quadratic (Kerr) effect is used, as in a nitrobenzene liquid cell for example, the phase difference introduced is proportional to the square of the applied voltage. The effective value of the half-wave voltage can then be reduced, in principle, by biasing the cell with a fixed voltage V_b and working between V_b and $V_{b+\pi}$.

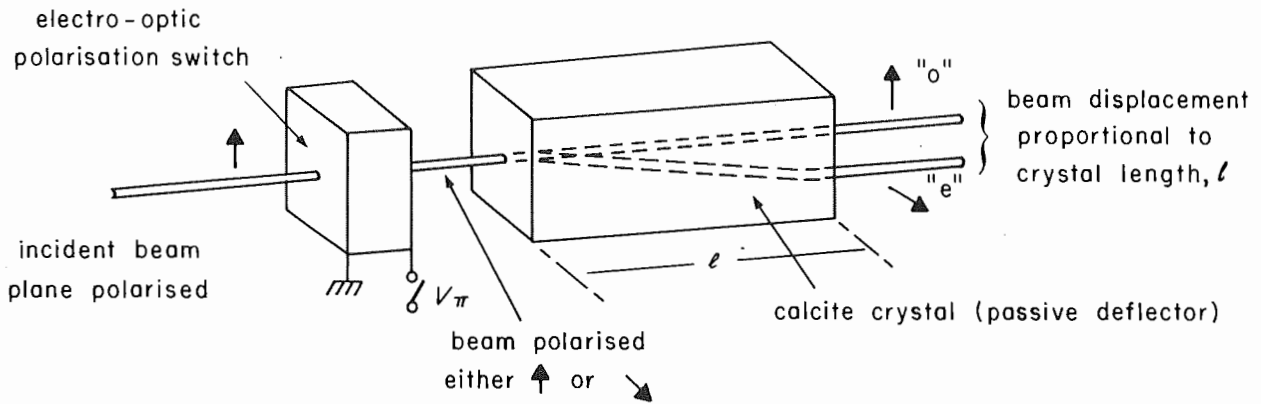
3.3. The digital light deflector

This device, which was briefly described in the previous section, is attractive for the particular hologram recording system envisaged. The digital light deflector is capable of directing a laser beam (or an array of beams) through a total of 2^N separate output positions by cascading N similar stages and it has the following intrinsic advantages:

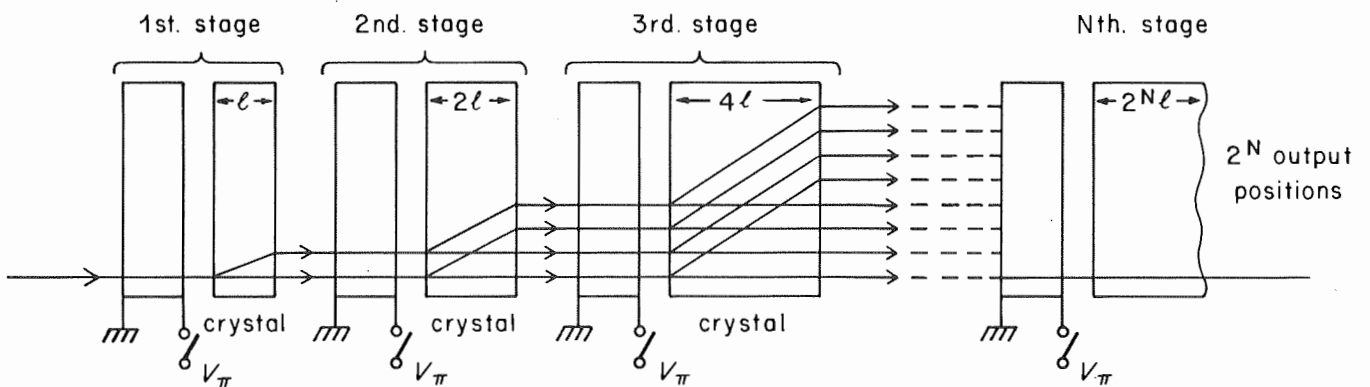
- (a) It is binary in concept and operation; each output position can be selected by a single N -bit address.
- (b) The geometry of the output positions is fixed rigidly by the prismatic construction of the passive optical elements.



(a)



(b)



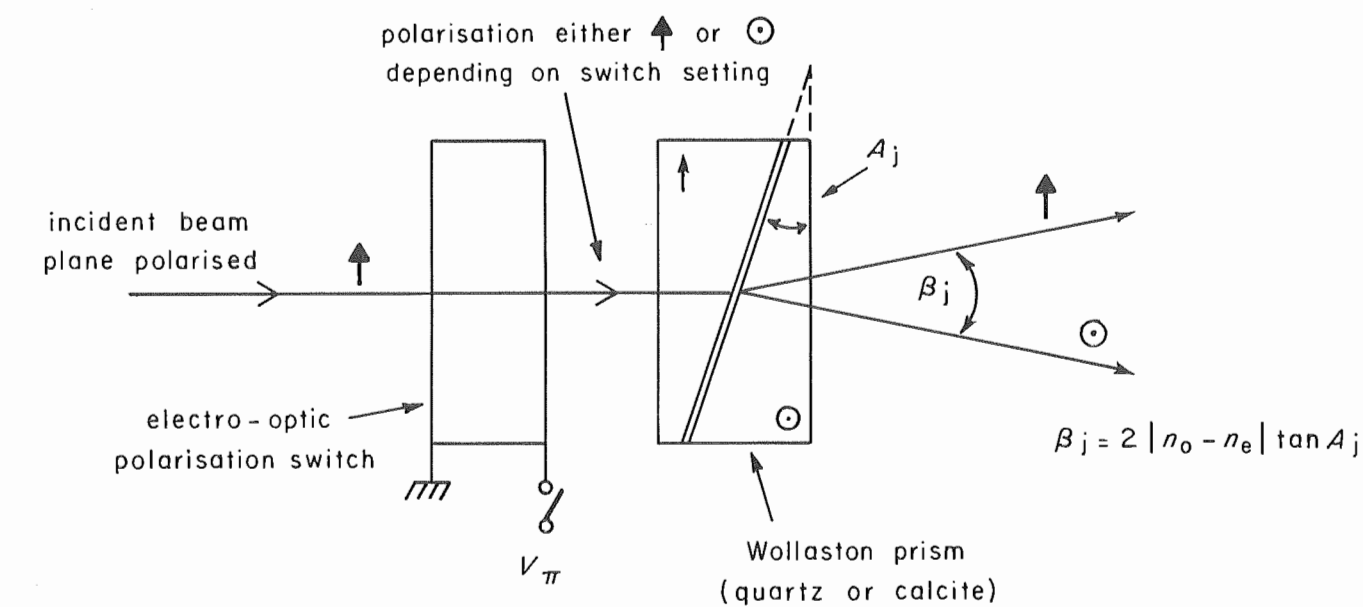
(c)

Fig. 4 - Electro-optic deflection

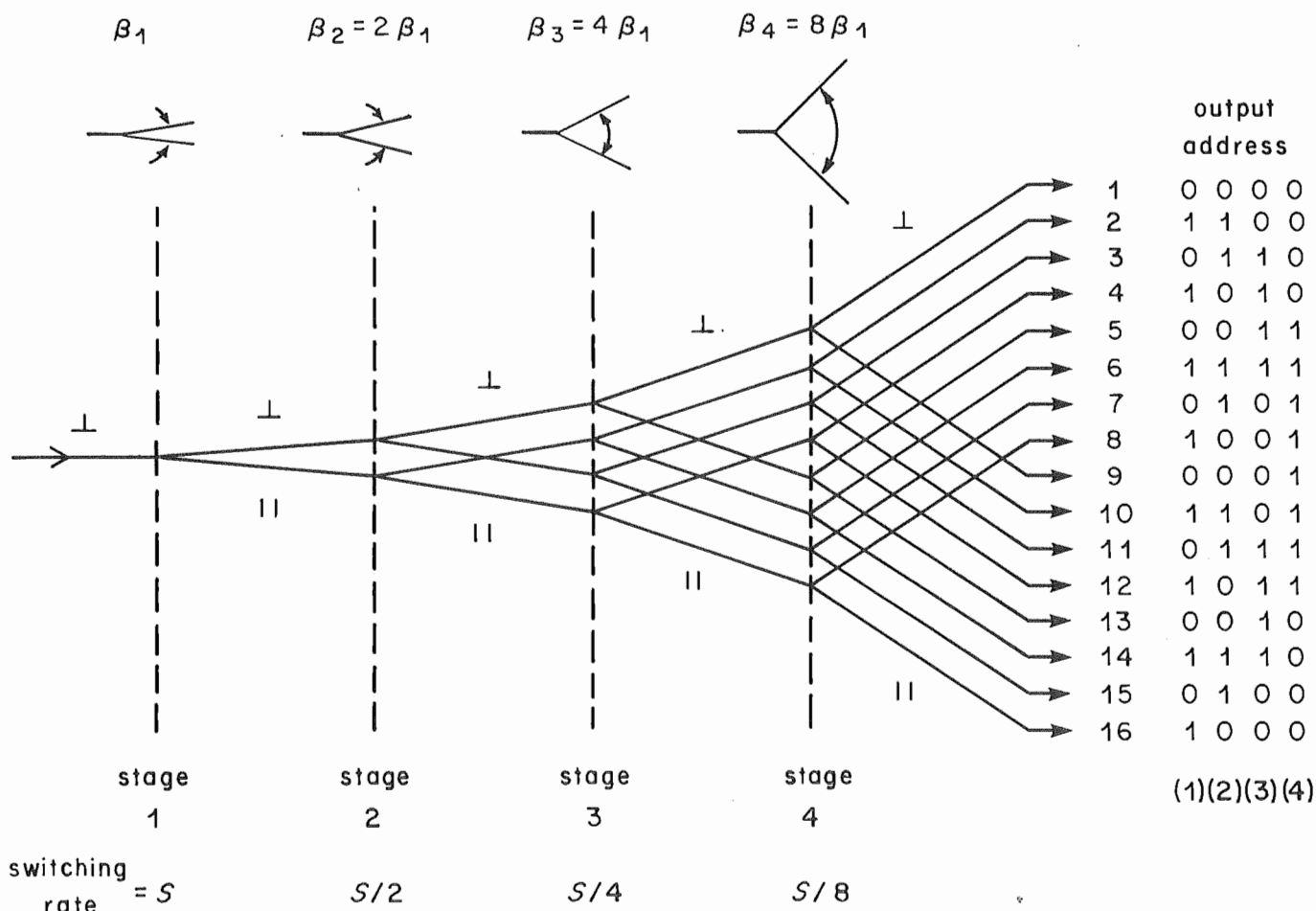
(a) analogue method using an electro-optic crystal prism

(b) digital arrangement combining an electro-optic polarisation switch with a passive birefringent crystal

(c) tandem arrangement forming an N -stage digital deflector



(a)



(b)

Fig. 5 - Digital deflection using Wollaston prisms to give angular separation of beams

(a) basic arrangement of each stage

(b) path structure and output addresses for a 4-stage Wollaston deflector with $\beta_{j+1} = 2\beta_j$

- (c) The emerging beam cross-fades from one angular position to the next (or any other); thus there is no actual motion of the focused spot, relative to the recording medium, caused by the deflection process.
- (d) The speed of deflection is limited only by the basic properties of the polarisation switches and the electronic circuits required to drive them. In a regular scanning application there is no flyback problem.
- (e) It is non-mechanical in operation.

The characteristics and construction of digital light deflectors has been reported in detail elsewhere.^{12,13,14} There are significant practical difficulties involved in their construction and, thus far, their development is only just emerging from the laboratory phase. From previous work, it would appear that if the application requires only a modest deflector capacity (up to 8 stages or 2^8 output positions, say) and a modest system aperture ($f/3$ or smaller), the development of an efficient and reliable device is feasible.

There are many parameters, some critical and some conflicting, involved in the design of a digital light deflector. These have been considered in some detail for the present application, which is to deflect a parallel array of 50 digit beams, plus a central reference beam, through 2^7 discrete angular positions in $64 \mu\text{s}$, with transition times better than 100 ns. (See Section 2.) A summary of the principal features of a suitable deflector using Wollaston prisms and KD*P polarisation switches, including the results of tests on experimental switches and prisms, is given below in Sections 3.3.1 to 3.3.3.2.

3.3.1. General characteristics

A typical stage of the deflector is constructed as shown in Fig. 5(a), where the Wollaston prism serves to produce an angular separation of β between the emerging rays. A tandem arrangement of deflection stages, in which it is arranged that $\beta_{j+1} = 2\beta_j$, gives rise to the path structure shown schematically in Fig. 5(b). A 4-stage deflector, as indicated in the figure, generates sixteen output positions and these have the binary addresses shown in the column on the right (a logic '1' indicates a half-wave voltage required and a logic '0' no-voltage required). It will be seen, from the address column in Fig. 5(b), that if each output position is to be occupied consecutively (regular scanning) then the logic state of two stages must be changed for each new position. The same scan of the sixteen output positions can also be obtained using a reversed arrangement of prisms in which $\beta_{j+1} = \frac{1}{2}\beta_j$, i.e. with the prism giving the largest

deviation in the first stage. The binary address sequence then has a Gray code characteristic in which the logic state of only one of the stages needs to be changed to arrive at the next scan position. This reversed arrangement therefore involves the least consumption of driving power, but there are optical penalties which are discussed later in this report.

If an irregular scan is acceptable, there are many other address sequences possible; referring to Fig. 5(b), for example, an address sequence with Gray code characteristics is the 'reflected' sequence, 1,16,2,15,3,14 etc. in which the output direction swings alternately either side of the system axis.

In a regular scanning arrangement, with $\beta_{j+1} = 2\beta_j$, the first stage is the fastest and is switching between states at a rate $S = \tau_1^{-1}$ times per second, where τ_1 is the dwell time allowed at each output position. (In the system under consideration $\tau_1 = 500 \text{ ns}$ so that $S_1 = 2 \times 10^6$ switches per second.) The switching rate for the j th stage is $S_j = 2^{(1-j)}\tau_1^{-1}$ and thus the drive control-waveforms comprise a synchronously phased set of square-waves with fundamental frequencies given by $2^{-j}\tau_1^{-1}$ ($j = 1, 2, \dots, N$) respectively.

The principal optical characteristics of the deflector are determined by the number of stages, the total deflection angle, the thicknesses and separations of the components, and the system aperture. In a Wollaston prism, the angular separation of the emerging rays is determined by the prism angle and the natural birefringence of the crystalline material. For small separation angles, the relationship is $\beta_j = 2|(n_o - n_e)|A_j$ where n_o and n_e are the ordinary and extraordinary refractive indices, respectively, and A_j is the prism angle (see Fig. 5(a)). However, β_j is not completely independent of the angle the incident beam makes with the system axis and, further, the ray deviations are not precisely symmetrical (i.e. not precisely equal to $\pm\frac{1}{2}\beta_j$). It will be seen that the maximum angle of incidence on the prism in the j th stage is less than $\frac{1}{2}\beta_j$. As a result of these prism aberrations (see Reference 14), the uniformity in the angular spacing of the output positions is perturbed. The effect is not serious (a few percent) in a low-capacity deflector with a total angle of deflection less than 10 degrees.

Fig. 6 illustrates the geometry of the output positions of an experimental (but incomplete) seven-stage Wollaston deflector arrangement; the photographs show an enlargement of a multiplicity of holograms ($\cong 60 \mu\text{m}$ diameter) formed by passing 38 parallel beams and a reference beam through the deflector with the polarisation switches replaced



Fig. 6 - The array of holograms obtained with an experimental (but incomplete) 7-stage Wollaston deflector

(a) 5th stage prism omitted
(b) 1st and 5th stage prisms omitted

by circular polarisers so that all the output positions are simultaneously illuminated. Fig. 6(a) shows the array formed with the 5th stage prism omitted and Fig. 6(b) with the 1st and 5th stage prisms omitted.

Another optical feature of prism deflectors is known as the 'walk-off' problem. Not only do the extreme angles of incidence increase as a ray progresses through the deflector but there is a lateral displacement of the ray from the system axis. This does not affect the geometry of the output positions in a Wollaston deflector, because the beams are collimated during transit and then finally brought to a focus with an external lens. It can, however, significantly increase the minimum required aperture of the final stages, and of the focusing lens, in the direction of deflection. The degree of 'walk-off' is a function of the total deflection angle, the number and arrangement of stages and the separation between the centres of the Wollaston prisms. Assuming a common prism spacing, l_p , (including that of the final lens) the minimum system aperture is increased by an amount less than $2l_p\beta_N$ (β_N in radians) for the arrangement $\beta_{j+1} = 2\beta_j$ (Fig. 5(b)). Clearly, the last stages contribute most to the 'walk off' effect so the design should aim to minimise the physical separation of the final prisms and focusing lens.

3.3.2. Polarisation switches

The most difficult problems arise with the design and construction of the polarisation switches, especially if the switching rates are in the megahertz region and the rise and fall times are to be less than 200 ns, as in the present requirement. This is true whether or not the electro-optic cells are constructed using liquids such as nitrobenzene or uniaxial crystals such as KD*P.¹⁵ It seemed that the latter electro-optic material was the most promising for the present application, even if not the one with the best figure of merit. More importantly, KD*P is commercially available in strain-free optical quality at a price which is not prohibitive.

The characteristics of a basal section cut from an APD (ammonium dihydrogen phosphate) crystal, and its use as an electro-optic shutter were examined by Billings.¹⁶ More recently KD*P crystals have been grown; this material has an identical crystal classification to ADP but its half-wave voltage is very much lower (due to the higher Curie temperature of KD*P).

The optical behaviour of an electro-optic crystal is complicated and a full description is beyond the scope of this report (see Ref. 16). Basically, a KD*P crystal behaves as a negative uniaxial crystal ($n_o > n_e$) when there is no electric field but becomes biaxial when a field is applied. Light propagates within the crystal either as an ordinary ray, with its electric vector perpendicular to the optic axis, or as an extraordinary ray polarised orthogonally to the ordinary ray. In a negative crystal, the phase velocity in the direction of propagation is greater for the extraordinary component. Thus, in general, there is a phase difference or retardation, ϕ , between the two components on emerging from the crystal, and light initially plane-polarised usually emerges elliptically polarised. The aim in an electro-optic

modulator or switch is to use the dependence of ϕ on the applied field in order to control the polarisation characteristics of the emerging light.

The simplest construction of a KD*P polarisation switch is shown in Fig. 7(a), where a slab of crystal is cut with the optic axis (Z axis) normal to the principal faces, and the edges parallel to the X and Y axes. In this 'longitudinal' type the light is directed along the optic axis, as shown, and the electric field is applied in the same direction. To achieve this field, the entry and exit faces are coated with optically transparent conductors, such as certain forms of tin oxide (or metal grids can be used) and these electroded faces are connected to a high-voltage source via an electronic switch. On application of the voltage, the ordinary and extraordinary rays propagating in the crystal have vibration directions at $\pm 45^\circ$ to the X (or Y) crystallographic axis, as indicated in Fig. 7(b) by the induced axes X' , Y' . Suppose under these conditions, that a plane polarised laser beam is directed along the Z -axis with its electric vector of unit amplitude parallel to the X axis of the crystal (Fig. 7(b)). Then, within the crystal, two components of amplitude $1/\sqrt{2}$ and vibrating along the induced axis X' and Y' respectively, are propagated. If the voltage is adjusted so that the total phase retardation introduced on traversing the crystal is 180° , (this is equivalent to writing $-1/\sqrt{2}$ for the amplitude of one component) the light is plane-polarised on emergence but its resultant electric vector has been rotated through 90° , as shown.

The induced phase retardation, ϕ , for a Z -cut longitudinal modulator is given by

$$\phi = 2\pi\lambda^{-1}n_o^3r_{63}El \quad (8(a))$$

Where E is the field strength, n_o is the ordinary refractive index, r_{63} is the appropriate electro-optic coefficient* and l is the crystal thickness in the direction of propagation. In terms of the applied voltage $V = El$.

$$\phi = 2\pi\lambda^{-1}n_o^3r_{63}V \quad (8(b))$$

which shows (a) the linear relation between the phase retardation and voltage and (b) that the phase retardation is independent of the crystal thickness for a given applied voltage. The half-wave voltage, V_π , is that required to induce a phase retardation of π radians, which from Equation (8(b)) gives

$$V_\pi = \lambda(2n_o^3r_{63})^{-1} \quad (9)$$

Note that the half-wave voltage is directly proportional to the optical wavelength. The coefficient r_{63} for KD*P is approximately 24×10^{-12} m/V the precise value depending on the completeness of the deuteration and the way the crystal is mounted or clamped. Typically, for an optical wavelength of 633 nm, V_π lies in the region of 4.5 kV.

* The electro-optic effect in crystals is a function of the direction of the applied field relative to the axes of symmetry. In general, a matrix of electro-optic coefficients r_{ij} are required to completely specify the effects. The suffix '63', attached to the coefficient r_{63} , denotes the position of the element in a commonly-used matrix specification.

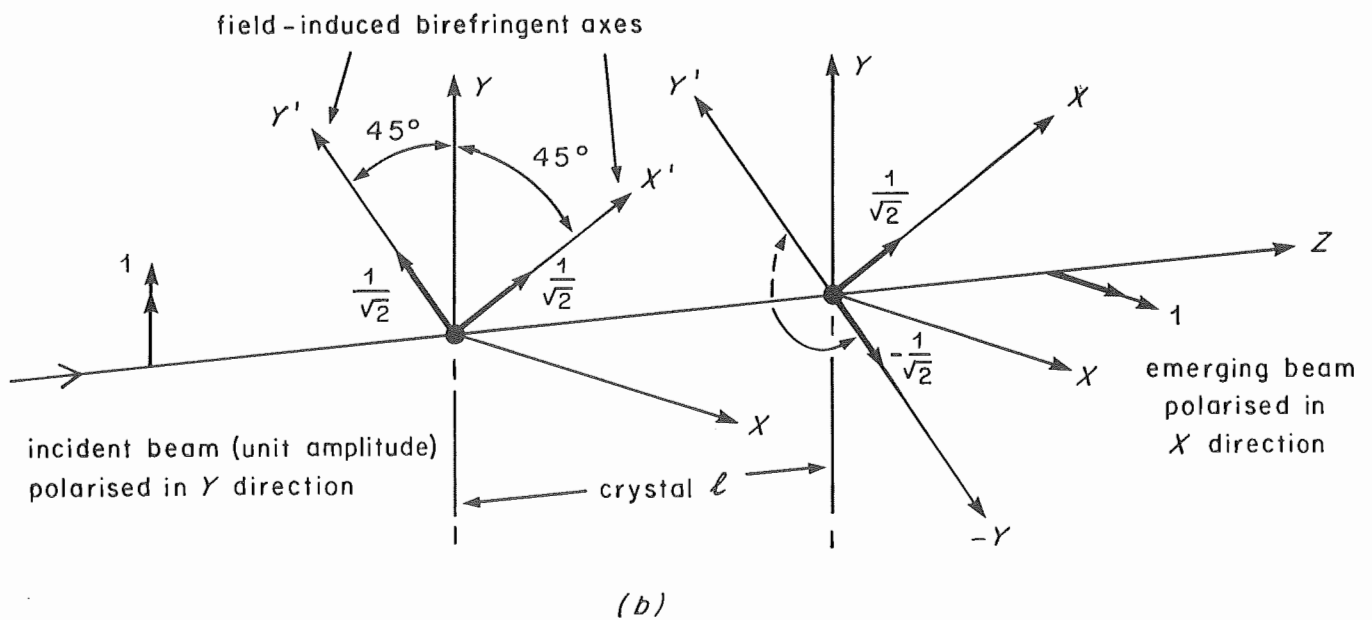
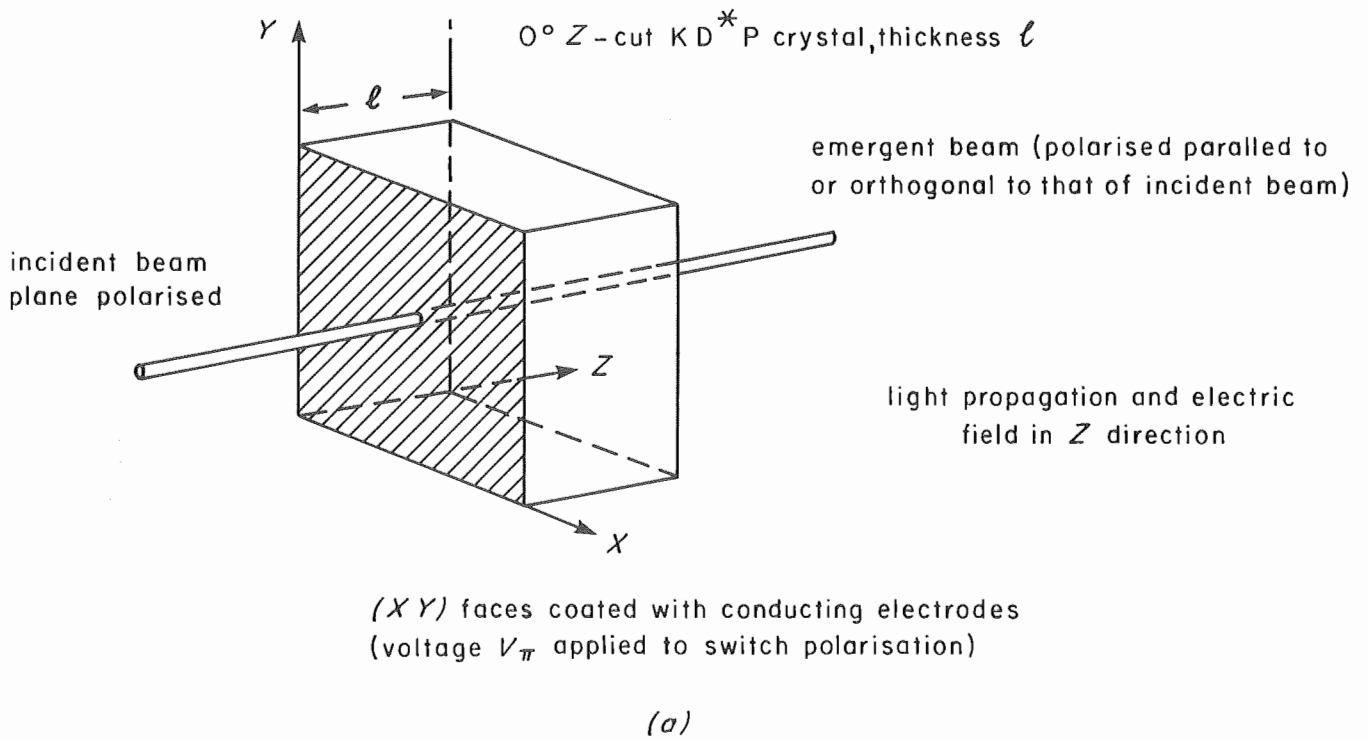
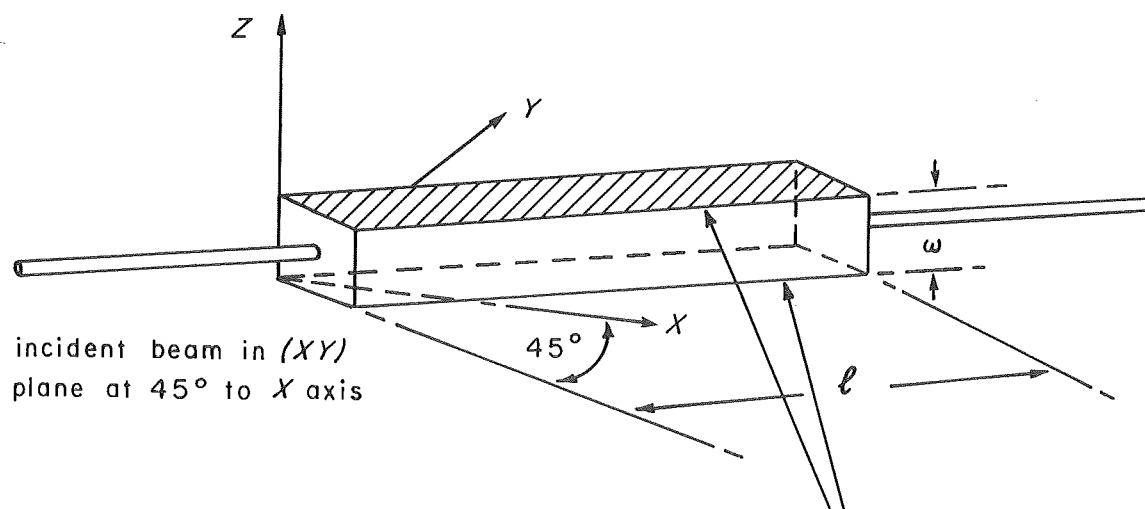
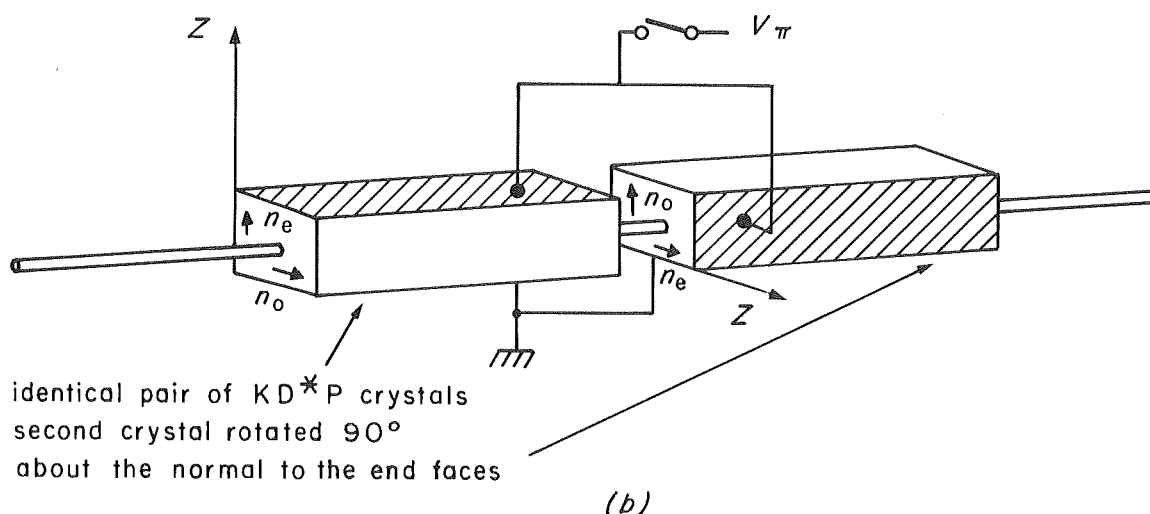


Fig. 7 - Longitudinal design of KD^*P polarisation switch
 (a) basic construction (b) electric vector diagram with half-wave voltage applied



45° Z cut KD*P crystal, length l , electroded Z faces;
electric field in Z direction

(a)



identical pair of KD*P crystals
second crystal rotated 90°
about the normal to the end faces

(b)

Fig. 8 - A transverse design of KD*P polarisation switch

(a) basic construction

(b) temperature compensated arrangement using matched pair of crystals with their Z-axes crossed

////// electroded faces

Fig. 8 shows the construction of a 'transverse' type of phase modulator which could also be used to form a polarisation switch for the deflector. In this arrangement (Fig. 8(a)) the electric field is applied in the Z-axis direction, as before, but the light propagates parallel to the (XY) plane at 45° to the X axis, and is therefore orthogonal to the electric field. The formula for the retardation of a single crystal of length l in the direction of propagation is then

$$\phi = 2\pi\lambda^{-1} [(n_o - n_e) + \frac{1}{2}n_o^3 r_{63} E l] \quad (10(a))$$

which is similar to that for the longitudinal arrangement (Equation 8(a)) except for the natural birefringent term $(n_o - n_e)$. Because the birefringent term is large and temperature dependent, it is necessary to cancel its effect

by using a second crystal of identical length, l , orientated as shown in Fig. 8(b). The ordinary ray, in the first crystal becomes the extraordinary ray in the second, and vice-versa; the principle is shown in Fig. 8(b). The total retardation of the composite crystal is, after substituting $E = V/w^{-1}$, where w is the separation of the electroded faces,

$$\phi = 2\pi\lambda^{-1} n_o^3 r_{63} V l w^{-1} \quad (10(b))$$

and the corresponding half-wave voltage is

$$V_\pi = \lambda (2n_o^3 r_{63})^{-1} w l^{-1} \quad (11)$$

Thus the advantage of a transverse design, in principle, is that the half-wave voltage can be reduced by increasing the

crystal length and/or reducing the electrode separation i.e. the aperture. However, in practice, composite crystal lengths greater than about 60 mm tend to be thermally unstable, so that for large aperture (20–30 mm) applications the possible reduction in half-wave voltage is not dramatic. Moreover, the crystal volume is then large. An important advantage of a transverse crystal design, especially for deflectors, is that the light does not pass through the electrode structures. This leads to a significant increase in the overall transmission of a multi-stage device, because there are no absorption losses at the crystal faces.

There are a number of design difficulties associated with crystal polarisation switches, and these need careful consideration if an efficient deflector is to be constructed. The principal problems are discussed below in Sections 3.3.2.1 to 3.3.2.3.

3.3.2.1. Optical switching efficiency

If plane-polarised light is incident on a switch in the deflector which is not operating perfectly the emerging light will be slightly elliptically polarised, so that a fraction of the output will be coupled into an unwanted direction. Calling this fraction g , we can define the optical switching efficiency as $(1 - g)$. The switching efficiency in large-aperture switches is impaired by natural birefringence, crystal inhomogeneity, acoustic standing waves induced piezo-electrically, spatial non-uniformity of the applied field and departures from the correct half-wave voltage. The effect of poor switching efficiency is that light appears in the recording plane at positions other than the one addressed. In the present application, this produces cross-talk between the recorded holograms. The total amount of wanted light reaching the addressed position is proportional to $(1 - g)^N$, for an N stage deflector with equal switching efficiency at each stage. Thus a quantity proportional to $1 - (1 - g)^N \approx Ng$ (for $g \ll 1$) must stray into other positions. It may be shown that in a complete scan of the 2^N positions with a beam of constant input intensity, the total amount of unwanted light is distributed uniformly over the scan. Thus, in this case, we have an integrated total proportional to $2^N Ng$ distributed over 2^N positions, which clearly leads to an average amount per output position proportional to Ng . The ratio of wanted to unwanted light per output position is thus approximately given by $[(Ng)^{-1} - 1] : 1$. To obtain a ratio better than 10:1 in a 7-stage deflector, for example, g must be less than 1.3%. One method of relaxing the tolerance on the switching efficiency is to add an extra stage to the deflector consisting of a fixed polariser preceded by a polarisation switch. The latter is cyclically switched so that the wanted light passes through the polariser but, simultaneously, the principal component of the unwanted light, which is always polarised orthogonally, is rejected. It can be shown that the average amount of unwanted light per output position is then proportional to $(Ng)^2/2$.

In the longitudinal form of switch, there is no natural birefringence for light incident normally on the (XY) faces i.e. propagating parallel to the optic axis (Fig. 7). However, for non-normal incidence, a single crystal introduces birefringence which can rapidly reduce the optical switching

efficiency. In a single-axis deflector application, using Wollaston prisms, there is a range of angles over which the light is incident at the various stages (except the first) but these angles are confined to one plane i.e. the plane of deflection. If the electric vector of the incident light is either normal to the deflection plane or lies in it, then the natural birefringence of the crystal with no field applied has little effect on the switching efficiency even for large angles of incidence. A proviso here is that the crystals must be accurately cut so that their optic axes also lie in the deflection plane. When the crystal is in the 'switched on' condition, i.e. with the voltage applied, the crystal becomes biaxial and the induced birefringent axes are ideally inclined at 45° to both the plane of polarisation of the incident light and to the deflection plane. A problem arises because the induced axes rotate from the ideal 45° orientation as the angle of incidence deviates from normality; furthermore, there is a change in the amount of induced birefringence with angle of incidence for which it is difficult to compensate.

Billings¹⁷ has discussed the various possibilities of switch construction which could relax this kind of angle limitation. The most effective way is to reduce the crystal thickness, but this solution is limited in practice by the fragility of KD*P crystals and the risk of electrical breakdown; minimum crystal thicknesses of about 2 mm are practicable. Another approach is to use two crystals of equal thickness with a fixed (i.e. passive) 90° polarisation-rotator sandwiched between them, as shown in Fig. 9. In order to prevent a nullification of the induced birefringence it is then necessary either to rotate the second crystal so that its X and Y axes are crossed (Fig. 9(a)), or to reverse the electric field in one of them as indicated in Fig. 9(b). A true 90° rotator suitable for monochromatic light can be realised with two half-wave plates (e.g. mica plates) in tandem but with their axes at 45° , as shown in Fig. 9(c).

Similar compensation arrangements have already been mentioned in connection with transverse types of switch, where there is a large natural birefringence even at normal incidence. These switches are even more sensitive to variation in the angle of incidence.

Deviations in the applied voltage from the correct half-wave voltage, V_π also impair the switching efficiency in the switched-on condition. For small deviations $\pm \Delta V$ from the required half-wave voltage

$$g \approx \left(\frac{\pi}{2} \cdot \frac{\Delta V}{V_\pi} \right)^2 \quad (12)$$

and this relation is shown in Fig. 10. The relative deviations in applied voltage ($\Delta V/V_\pi$) must be held to within $\pm 6.4\%$ in order to maintain $g \leq 1\%$. Care must be taken also in the electrode design to ensure a spatial uniformity of applied field.

3.3.2.2. Piezo-electric effects

Perhaps the most troublesome feature of crystal polarisation switches, in a cyclical switching application,

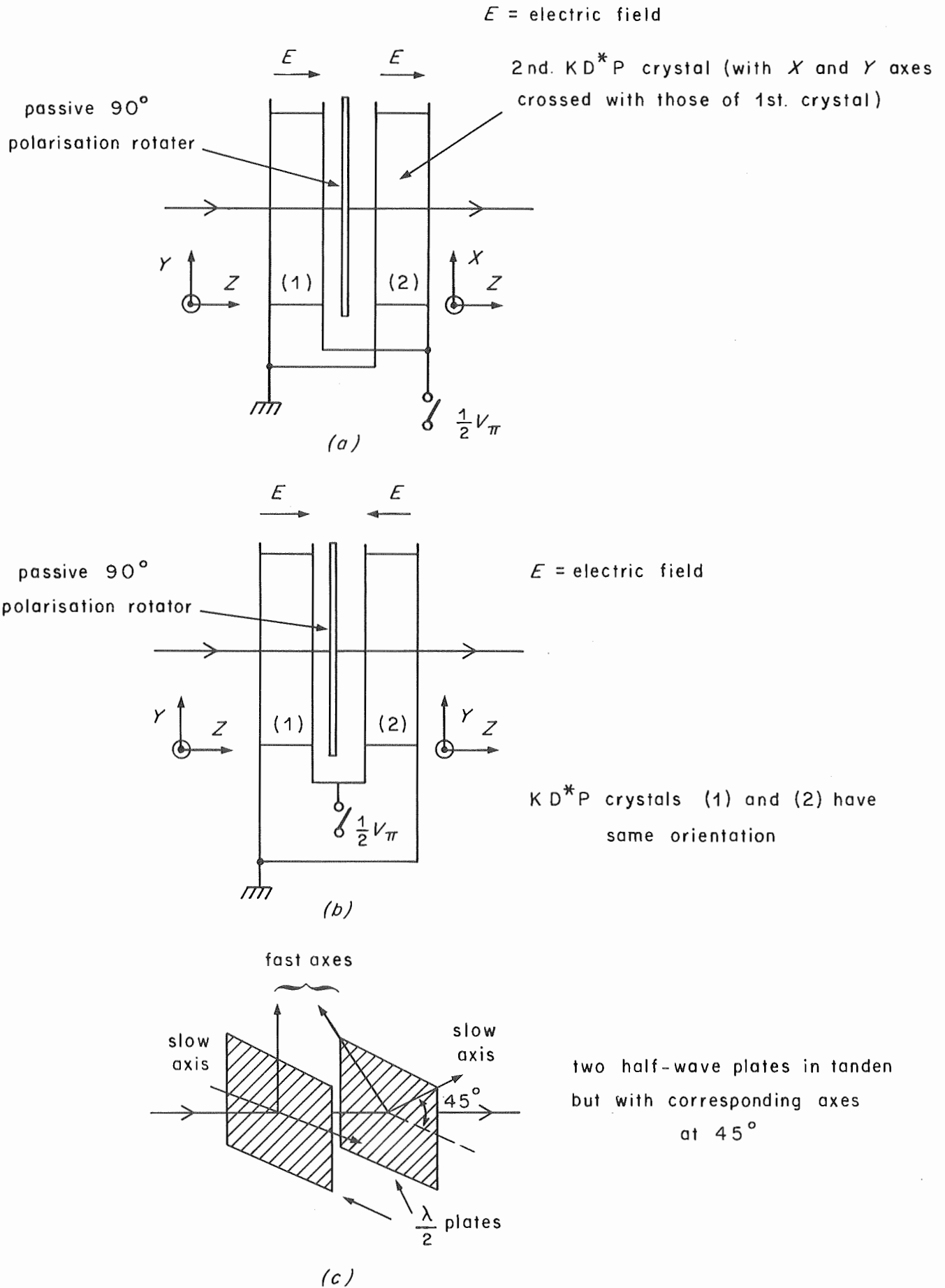


Fig. 9 - Methods for improving the angular field in longitudinal designs of KD^*P polarisation switches
 (a) crossed-axes arrangement (b) reversed-field arrangement (c) a passive 90° polarisation rotator

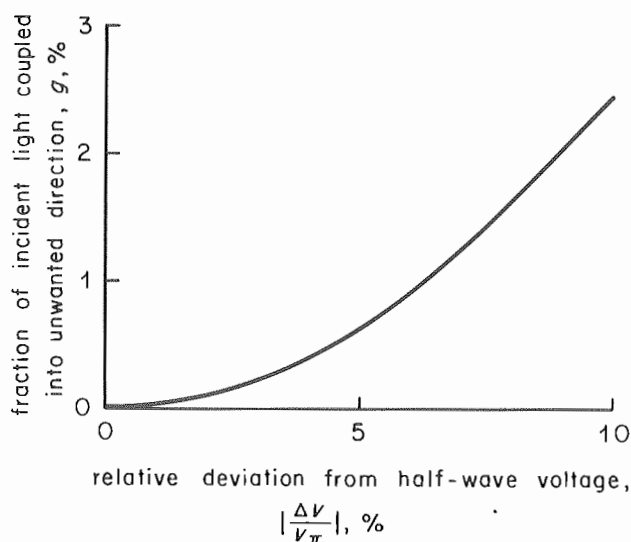


Fig. 10 - Effect of deviations from the correct half-wave voltage on the switching efficiency of a KD*P deflector stage

arises from the bulk acoustic wave motions induced by piezo-electric coupling. In longitudinal switches, it has been shown¹⁸ that standing shear-wave modes can be excited up to very high orders of resonance, with little diminution of amplitude in unclamped crystals. The effect is to cause spatial and temporal variations in the effective birefringence over the aperture corresponding to the complicated mode patterns set up.

The Equation (8(b)), derived earlier for the phase retardation in a longitudinal (Z-cut) design, contains the electro-optic coefficient r_{63} . However, if the crystal is not rigidly clamped and therefore allowed to strain mechanically via the piezo-electric effect, this coefficient is effectively increased and can be represented by

$$r'_{63} = r_{63} + \eta(\omega) \quad (13)$$

where r'_{63} is the modified electro-optic coefficient in the strained state and $\eta(\omega)$ is the added contribution due to strain. The contribution $\eta(\omega)$ can be relatively large at nodal areas when the angular frequency, ω , of the applied voltage is such as to create standing shear-waves within the

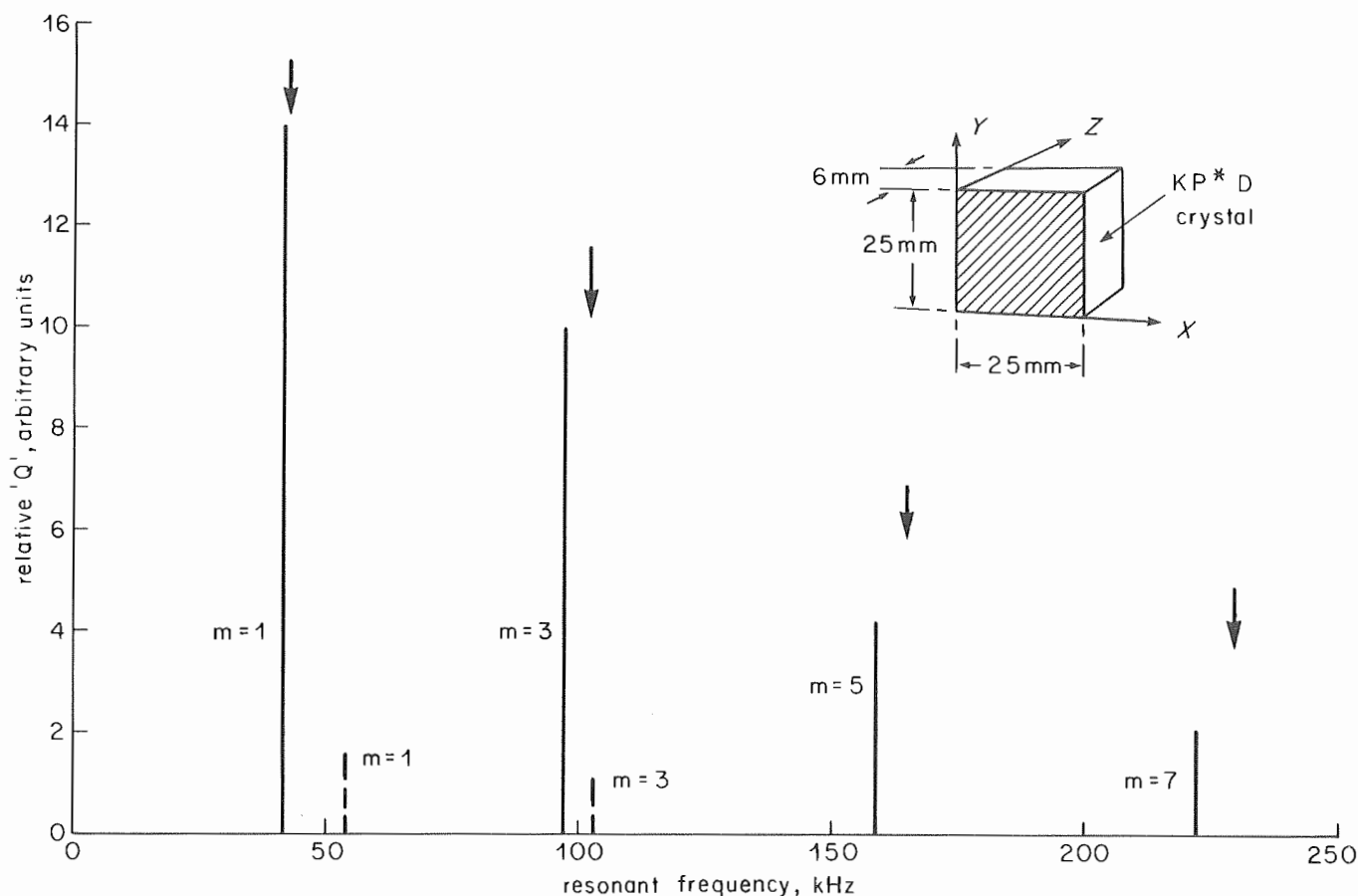


Fig. 11 - The shear-wave resonance structure in a KD*P crystal of size shown inset

— loose contact electrodes } measured values
 --- cemented unit }
 ↓ calculated frequencies of resonances in unclamped crystal

crystal. The effective half-wave voltage (given by putting r'_{63} in Equation (9)) then varies systematically over the crystal aperture according to the two-dimensional mode pattern set-up. From zero up to near the fundamental frequency (ω_1), the strain contribution gives a useful reduction in the half-wave voltage with substantial uniformity over the aperture. At higher orders of resonance, the spatial and temporal variations in V_π due to the mode pattern are troublesome in a multi-beam application.

Fig. 11 shows the measured resonances of a 0°Z -cut, $25 \times 25 \times 6$ mm, KD*P crystal; the ordinate values represent the relative ' Q ' of the various orders. The solid lines refer to the crystal with very loosely attached electrodes (i.e. virtually unclamped condition), while the dashed lines refer to the same crystal with a 1 mm glass plate cemented to each face. Also shown in Fig. 11, by the arrows, are the expected frequencies of the resonances in an unclamped crystal calculated from the following formula for a slab with XY faces of side d :

$$\omega_m = \pi d^{-1} v_{xy} m [1 + 8(\pi^2 m^2)^{-1} - 16(\pi^4 m^4)^{-1}]^{1/2} \quad (m = 1, 3, 5, 7 \text{ etc.}) \quad (14)$$

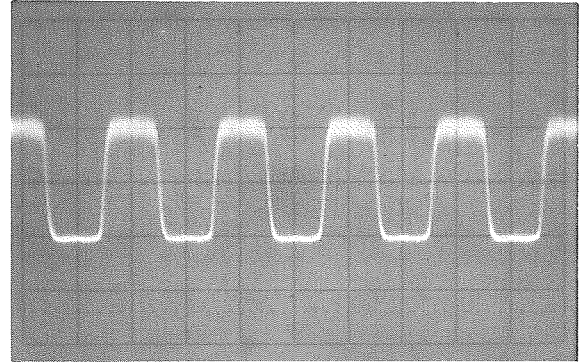
where $\omega_m = 2\pi$ times the resonant frequency (order m) and v_{xy} = the shear-wave acoustic velocity in the crystal; ($v_{xy} = 1.626 \text{ km.s}^{-1}$ for KD*P). Equation (14) is derived¹⁸ from the theoretical shear-wave solutions¹⁹ for a slab with square (XY) faces. It will be seen from Fig. 11 that the lower-order resonance frequencies are not precisely harmonically related to the fundamental ($m = 1$); the spacing between resonant frequencies becomes more constant as the order increases. In the partially clamped condition, it appears that the resonant ' Q ' values are dramatically reduced, especially of the higher orders and, also, the frequency of the fundamental is significantly increased, presumably due to a modification of the elasto-optic coefficient.

The basic parameter controlling the resonant frequency structure is the lateral size of the crystal, i.e. the dimensions of the (XY) face. There are, therefore, three principal methods which can be used to mitigate any undesirable piezo-electric effects. These are:

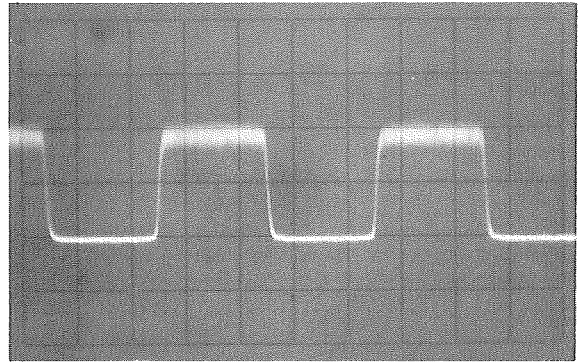
- (a) To select a crystal size such that the fundamental frequency is substantially higher than that of the switching waveform.
- (b) To select a crystal size such that the resonant frequency structure interleaves with the switching waveform spectrum.

and (c) To rigidly clamp the crystal faces so that surface strain is prevented.

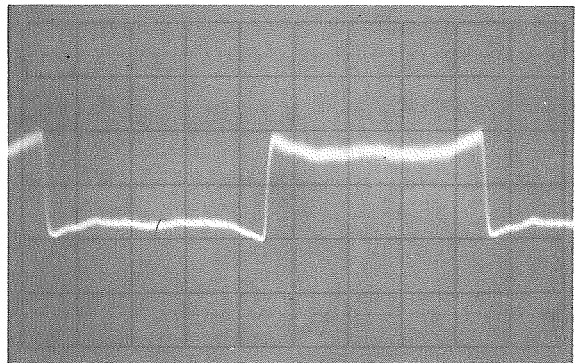
In the envisaged recording applications, crystal apertures not less than 18×18 mm are required in the deflector; this leads to a fundamental resonance frequency of about 70 kHz. However, the required set of square-wave voltage waveforms have fundamental frequencies varying, in octave jumps, from approximately 16 kHz for the slowest stage,



(a)



(b)



(c)

Fig. 12 - Performance of a KD*P polarisation switch as the fundamental (square-wave) frequency of the applied electric field is varied

(a) 250 kHz (b) 125 kHz (c) 62.5 kHz

Note waveform distortion in (c) due to piezo-electric resonance effects.

to 500 kHz for the fastest stage. Thus solution (a) above is not compatible with these requirements. Solution (c) would be ideal but it seems unlikely that clamping can completely suppress the lowest-order resonances, bearing in mind the high switching-voltages required. (In this respect it should be noted that the piezo-electric contribution in KD*P is lower than other crystals of this class, such as ADP, i.e. $r'_{63} - r_{63}$ is measured to be the lowest.) Thus, after clamping the crystal as well as possible (e.g. by cementing glass plates to the surfaces) it is important to make sure that at each stage the crystal resonance spectrum interleaves with the applied voltage spectrum, at least over the lower orders.

In a typical design situation, a square-wave type of voltage waveform is applied and its spectrum will consist of the fundamental and odd-order harmonics, with amplitudes weighted inversely by the order of the harmonic. The fundamental frequencies, however, vary from stage to stage in the deflector (octave steps) so that it may not be possible to find a common crystal size for all stages. This is illustrated in Fig. 12, which shows the 'optical' switching responses obtained with an experimental crystal switch as the fundamental frequency of the applied square-wave voltage is lowered from 250 kHz in octave steps. It will be seen that, at the highest switching frequencies, Figs. 12(a) and (b), the output is substantially free of piezo-electric coupling effects. At the lowest frequency, Fig. 12(c), coupling has occurred and the waveform is severely distorted. It is clear that for this stage the crystal face dimensions must be adjusted to improve the spectral interleaving.

3.3.2.3. Electroding

Transverse switches can use thick metal plates either held in direct contact or cemented on to the transverse faces. A gold interface between plate and crystal is often used to prevent electrolytically formed surface deposits and to reduce metal-ion migration, the plates usually form part of the support structure for the crystal.

In longitudinal switches, a conflict arises between the need to have low-resistance electrodes and, at the same time, low optical transmission losses. If the switching waveform is unipolar and has a direct current bias, it is also necessary to form the electrodes directly on the crystal surfaces, in intimate contact, to prevent the build-up of charge barriers. An attractive solution is to deposit a layer of conducting tin-indium oxide directly on to the surface. Vacuum deposition using r.f. sputtering techniques can produce highly transparent oxide layers with resistances of several ohms per square.* Tin-indium oxide layers have high refractive indices (≈ 2) and therefore need to be about one half-wavelength in optical thickness to eliminate reflection losses when the cell is finally immersed in an index-matching liquid or cement. The optical transmission is high in the red part of the visible spectrum but there can be up to two percent absorption in the blue region. In a seven-stage deflector with four electroded surfaces per stage, for example, a 2% absorption/reflection

* Switch failures have been reported with this type of electrode, which is believed to be due to metal-ion migration into the crystal.

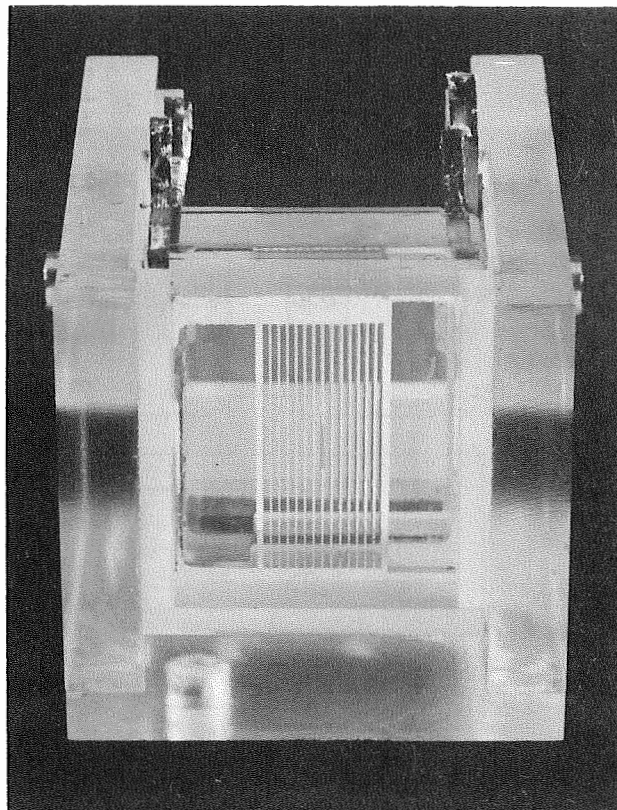


Fig. 13 - An experimental KD*P polarisation switch for a digital light deflector

loss per electrode means a total transmission loss of $1-(0.98)^{28}$ or about 43%, which makes the deflector rather inefficient.

An alternative electroding arrangement suitable for the recording application, in which an array of 50 discrete, but parallel beams is to be deflected, is to use a ladder electrode grid. A grid of this type is seen in Fig. 13 which shows an experimental KD*P polarisation switch. The array of beams passes through the slots (1 mm wide) in the electrode and the slots are aligned with each other and with the deflection plane. The ladder grids are formed by evaporating metal through an open mask held in close contact with the crystal surface. The field is not so uniformly distributed as with the conducting oxide layer but this is not serious if the crystal thickness is more than about three times the width of the slot. A greater disadvantage in this approach is the precision required in aligning the successive grid structures in the deflector and in the collimation of the input beams. However, if alignment is accomplished, the optical transmission is expected to be as high as that achieved in transverse designs.

In a typical KD*P switch operating at a switching rate of 1 MHz, the average displacement current flowing through the electrodes is of the order of 100 mA, and the resistive power dissipation in the electrodes is therefore about 10 mW per ohm. At this switching rate, the effective electrode resistances should be kept below 10 ohms to avoid adding significantly to the heat generated by the dielectric loss (see below).

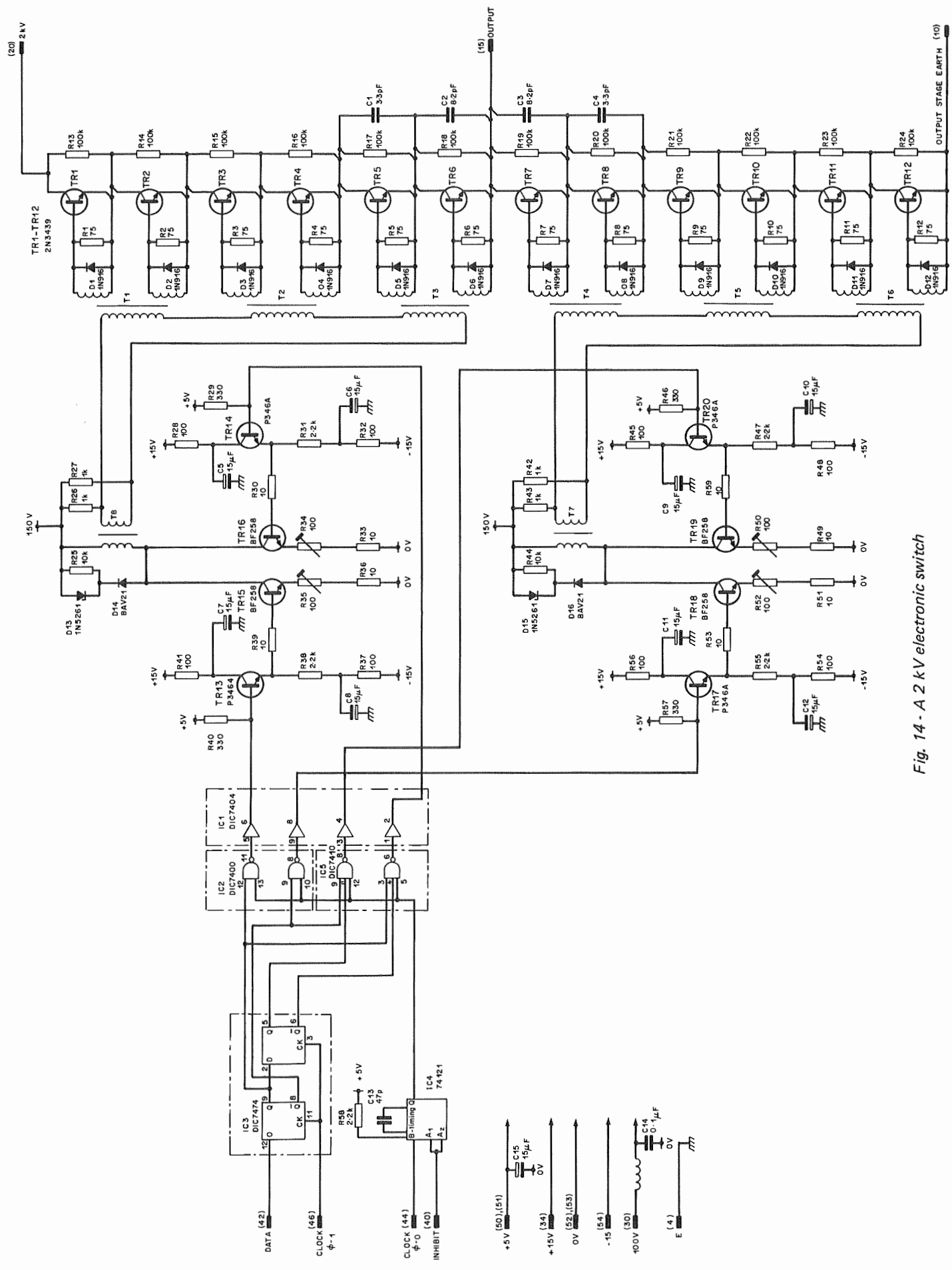


Fig. 14 - A 2 kV electronic switch

A further problem found with ladder grid electrodes when the crystal switch is driven with a unipolar voltage (from 0 to V_π volts, for example), is a build-up of residual charge on the surface of the crystal in the gaps of the grid. This can cause a significant, unwanted electrical bias if the surface conductivity of the crystal is very low. An obvious remedy is to use bipolar switching with a zero direct-current component ($-V_\pi/2$ to $+V_\pi/2$) but this then requires an added optical retardation bias of $\pi/2$ radians, i.e. a quarter-wave ($\lambda/4$) retardation plate combined with the switch. Another possible solution would be to increase the surface conductivity by using a suitable cement for the clamping plates or by evaporating an extremely thin coating of indium oxide overlaying the grid structure and gaps.

3.3.2.4. Thermal effects

Crystal switches are affected by temperature changes in a number of ways. Both natural and induced birefringences are functions of temperature because of the slightly different temperature coefficients for the ordinary and extraordinary refractive indices. Further, the elasto-optic constants vary slightly with temperature, so that piezo-electrically induced resonance structures may drift in frequency as the crystal becomes warmer.

In a digital light deflector, some rise in crystal temperature is inevitable after switch-on partly due to power dissipation in the electrodes, as mentioned earlier, but mainly to heating within the crystal from dielectric losses.

For KD*P the dielectric loss tangent is about 10^{-2} , so that for a crystal switch working at a total reactive power of 100 W for example, there is an internal power dissipation of one watt. The dielectric power dissipation per unit volume can be reduced by using a thicker crystal but, in longitudinal switches, this advantage is offset somewhat by the longer interaction path. It appears that thermal effects limit the maximum switching frequency of wide-aperture crystals to about 10^6 transitions per second.

3.3.3. High-voltage switches

A number of possible switching configurations suitable for square-wave operation of electro-optic polarisation switches (longitudinal form) were discussed by Lee,²⁰ who also gave circuit details of a fast electronic switch.

In an experimental longitudinal form of polarisation switch, the double-crystal approach, shown in Fig. 9(b), has been adopted in which the applied field direction is reversed in the second crystal. Using KD*P crystals, the switching voltage required is between 1.5 and 2.2 kV depending on the optical wavelength and the degree of deuteration. A 2 kV electronic switch has been developed capable of operating at rates of up to 10^6 transitions per second. The complete circuit used is shown in Fig. 14; it is a modification of the one given by Lee and is described more fully in the Appendix.

The output waveform obtained with the switch is shown in Fig. 15; the regular bumps in the trace are due to the mode of operation of the circuit and are entirely normal.

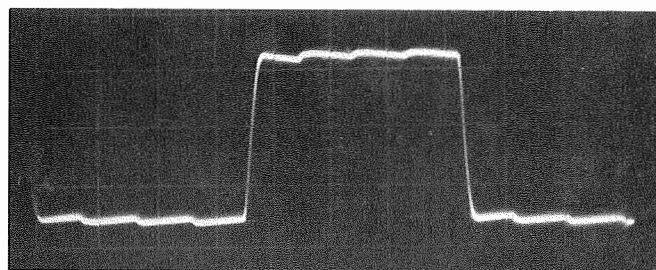


Fig. 15 - Output voltage waveform from the 2 kV electronic switch

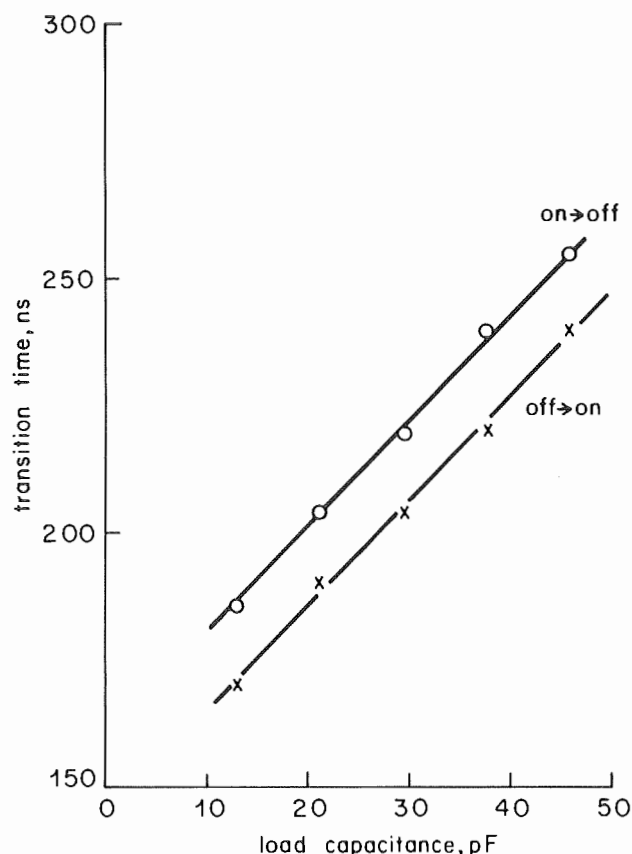


Fig. 16 - Switch transition times as a function of the load capacitance

Transition times are a function of the load capacitance, as indicated in Fig. 16, which shows the measured rise and fall times for a range of load capacitances. For a typical load of 22 pF, the transition times are approximately 200 nanoseconds.

4. Hologram page composers

4.1. General considerations

As mentioned previously, one of the main components of a holographic recording system is the page composer. This is an array of light modulators which intercepts an expanded laser beam and forms the set of digit beams to be recorded. A typical digit-beam pattern would be as shown

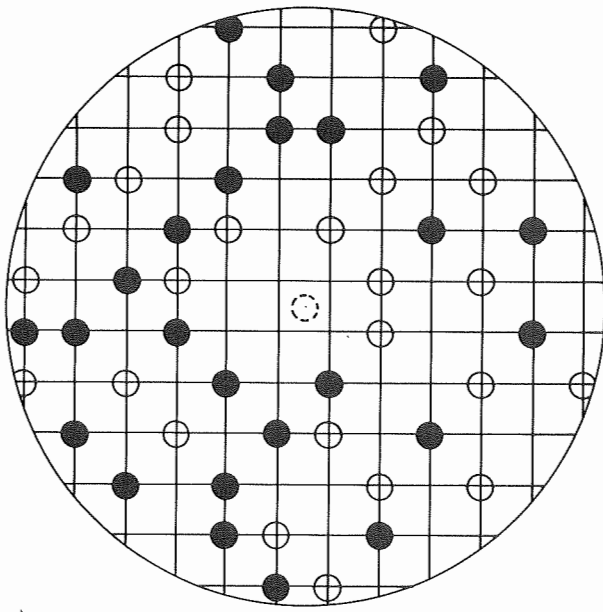


Fig. 17 - A typical page-composer pattern of digit beams
 ○ modulator positions ('0' state) } randomly scattered
 ● modulator positions ('1' state) } on lattice of possible positions

in Fig. 17, which represents an arbitrary 'page' of information containing 50 bits of binary data.

The general requirements of such a page composer have already been outlined (see Section 2). First, it must be able to cope with a total input data rate of 100 Megabits per second; for a composer consisting of 50 individual modulator ports, each individual port must therefore operate at 2 Megabits per second. Secondly, it should be of reasonable optical quality. Although the page composer would probably be followed by a spatial filter to reduce the effects of scattered light, any reduction of optical quality will lead to a corresponding reduction in optical efficiency. Thirdly, it should not be expensive and should be easy to drive with electrical signals.

There are many ways of modulating a light beam, but just as with the deflector, two of the possible methods are superior to the others. They are the acousto-optic and the electro-optic methods; the basic properties of both these methods are the same as those discussed in the context of deflection.

The acousto-optic method uses the device already shown in Fig. 3 and discussed in Section 3.2.1. The deflection of a light beam passing through an acousto-optic cell is a function of the frequency of the acoustic wave; in addition, the intensity of this deflected beam is a function of the amplitude of the acoustic wave. The expression relating the light intensity (I_2) emerging from the cell to the incident light (I_1) and acoustic wave power (P_{ac}) is:

$$I_2 = k_1 I_1 \sin^2 [k_2 (P_{ac})^{1/2}] \quad (15)$$

where k_1 and k_2 are constants.

Thus an acousto-optic deflector, in addition to causing deflection, can produce modulation of the light. Furthermore because the acoustic waves travel through the medium with finite speed, there is a degree of storage in the material and thus, in theory, a series of acoustic signals can be sent, one after the other, corresponding to a set of light beams. These acoustic waves propagate across the interaction aperture until each separate signal has reached the place corresponding to the light beam it is designed to modulate. At this instant the laser is flashed briefly, and each beam is modulated by the appropriate section of the composite acoustic wave; thus one modulator may control several beams.

In practice, it would be difficult to achieve the required resolution to both modulate and deflect several beams at once. Even using 50 separate acoustic cells, there would be considerable problems with pulsing the laser at the high repetition rates involved. In addition the system becomes rather expensive and difficult to drive (some 100–200 watts of swept r.f. power would be required).

For the above reasons it seems preferable to use variable birefringence electro-optic methods for the modulators. If an electro-optic polarisation switch (see Section 3.3.2) is sandwiched between two crossed polarisers, the combination forms an intensity modulator, as shown in Fig. 18. Under these conditions, with no applied voltage, the light beam is blocked by the relative orientation of the two polarisers. When an electrical signal is applied, the polarisation switch rotates the polarisation of the light through 90° so that it is then parallel to the axis of the second polariser and is therefore transmitted.

4.2. Electro-optic materials

There are many different electro-optic materials which can be used to make a modulator.²¹ Crystals which exhibit a linear (Pockell's) electro-optic effect are, for example, the ammonium dihydrogen phosphate (ADP) series already mentioned. These have good optical properties but the voltage drive requirements are high when used in the longitudinal mode. When used in the transverse mode for single-beam applications the half-wave voltages can be greatly reduced (100V to 300V instead of 4kV for

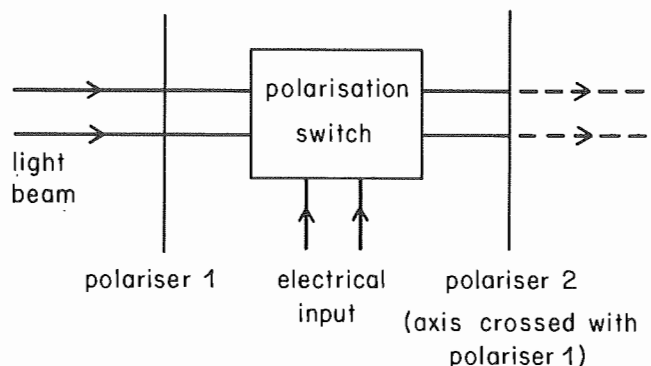


Fig. 18 - A single electro-optic modulator arrangement

KD*P), but two crystals must be used to compensate for the large natural birefringence (see Fig. 8(b)).

Other crystal materials such as lithium niobate, lithium tantalate and potassium tantalate-niobate are difficult to grow in the optical quality required and can be subject to damage in high intensity optical beams. However, they do have good electrical sensitivity.

There are also liquids such as nitrobenzene. Nitrobenzene is, however, highly toxic and requires electric fields of at least 35 MV/m; at these high fields, the liquid must be extremely pure to avoid trouble due to conductivity.¹⁵ Further, being liquid, there are problems with thermal convection currents. From an engineering point of view, solid interactive media are generally preferred.

Finally there are the electro-optic ceramics such as PLZT, which is an inexpensive, hot-pressed material. In contrast to the crystal materials, which have to be cut in a particular plane and used in a particular orientation, PLZT has no preferred direction. Moreover, for the high-lanthanum materials to be discussed later, the individual particles are of cubic crystallographic structure in the 'depoled' state. This means that the material is optically isotropic in the absence of an electric field and therefore has no natural birefringence. PLZT does have some disadvantages. It has hysteresis in its voltage/birefringence characteristics and it is not optically perfect (it is slightly translucent), but the imperfections are slight in well-polished thin slices. PLZT is, however, more sensitive than most of the crystal materials* and it is easier to fabricate electrodes on PLZT, as the ceramic does not dissolve in the dilute acids and organic solutions used.

For these reasons, viz. sensitivity, cost and ease of handling, PLZT was selected as the most suitable material for constructing an experimental 50-port page composer.

4.3. Characteristics of PLZT

PLZT is the name given to a family of electro-optic ceramic materials; the initials stand for lanthanum-doped lead zirconate-titanate. The material is a solid solution of lead titanate in lead zirconate, formed by hot pressing a mixture of lead, titanium and zirconium oxides. Small amounts of lanthanum oxide added to the original mix significantly affect the final properties of the ceramic. The material is non-absorbing in the visible spectrum, hard and very brittle; it is normally used in thin slices which are optically polished, and then mounted on a suitable substrate. The refractive index is high (up to 2.7) so that anti-reflection coatings are necessary for high transmission efficiency.

PLZT, is, in most of the common forms, ferroelectric (but see below and Ref. 22). This is analogous to the ferromagnetic properties of iron in that there exist, in the bulk

material, domains which are charged in a given direction. On a macroscopic scale, however, the random orientation of these domains causes no net charge to be present on the surfaces of the ceramic; this is referred to as the depoled state. When an electric field is applied the domains which are favourably oriented grow at the expense of the others and the material absorbs charge.

The charge density versus applied field characteristic shows a hysteresis loop due to this domain activity; the average relative permittivity is also high (in the region 2000 to 5000). The most common materials have a Zr/Ti ratio of 65/35. In these materials, if the percentage doping of La is less than about 8 atomic percent the hysteresis loop is square in shape. The material is therefore capable of storing information in an analogous way to a ferrite ring.

As the temperature is raised, the hysteresis loop closes up until the PLZT enters a 'slim-loop' condition; the

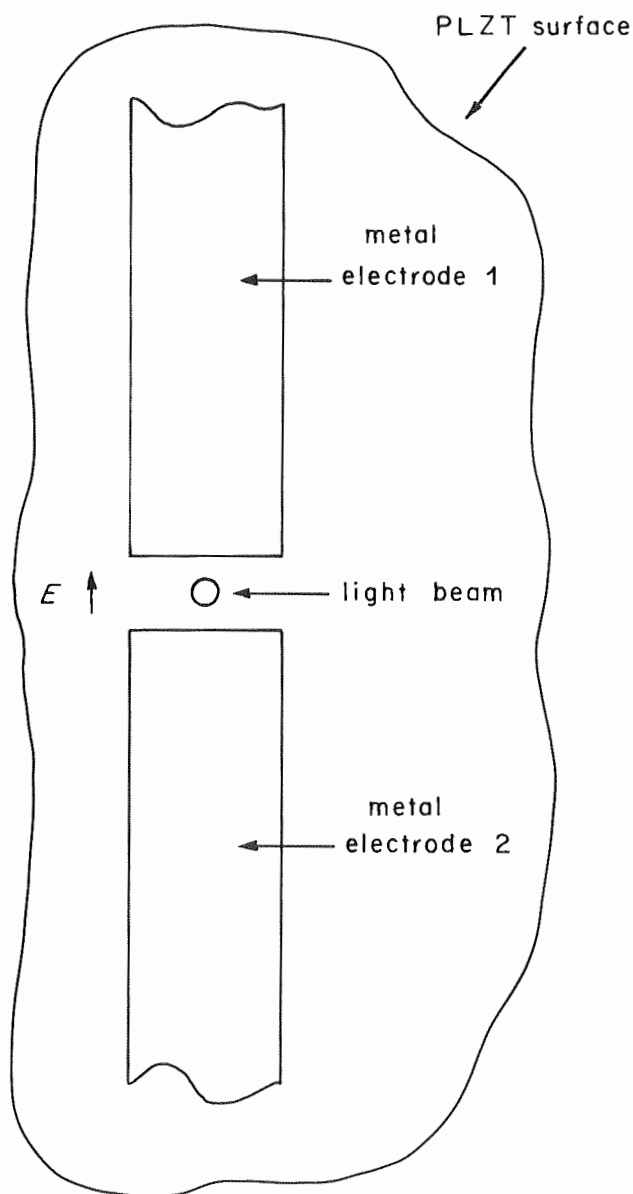


Fig. 19 - Electrode arrangement for a single modulator on PLZT

* The transverse electro-optic coefficient (change in refractive index, Δn) for PLZT, from Reference 22, is $0.0166 \text{ m}^4/\text{C}^2$. This is equivalent to about $0.015 \times 10^{-12} \text{ m}^2/\text{V}^2$ using the dielectric constant of PLZT.

temperature at which this gradual transition takes place is decreased as the lanthanum content is increased. When the lanthanum content is more than 8.5 atomic percent, the PLZT is in its slim-loop condition at room temperature. In this condition the material is non-ferroelectric in the absence of an applied electric field (see Ref. 22). This non-ferroelectric state becomes meta-stable below the slim-loop transition temperature band and can exist until the first application of an electric field. Thus, for a low-lanthanum material the so-called thermally — depoled and electrically — depoled states are not the same.

Light modulation may be achieved in two ways. The first is by using the electrically-variable scattering properties of low-lanthanum PLZT.^{23,24} For the application considered here, low-lanthanum PLZT is of little use because of the amount of heat generated by excusing the large hysteresis loop. The other way of achieving modulation is by using the variable-birefringence electro-optic effect. Metal finger electrodes are deposited on one side of the PLZT as shown in Fig. 19. Applying a voltage between the fingers causes a field, E , to be produced in the PLZT. This in turn causes the material to become birefringent. The birefringence is dependent on the orientation of the domains and is thus related to the absorbed dielectric charge field, D . The relationship is

$$\Delta n = k_1 D^2 \quad (16)$$

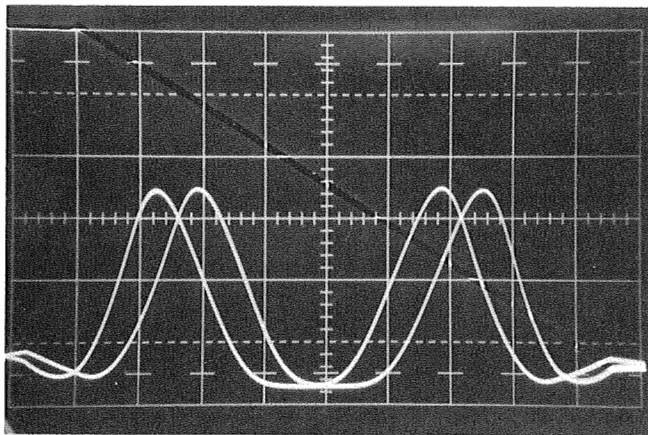
where Δn is the birefringence and k_1 is a constant. The intensity of the emerging light is related to the birefringence by

$$I_2 = k_2 I_1 \sin^2(k_3 \Delta n) \quad (17)$$

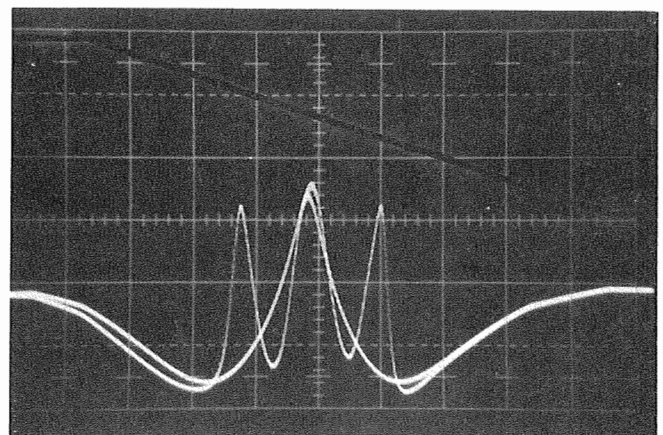
where I_1 is the incident intensity and k_2 and k_3 are constants.

Thus, from Equations (16) and (17),

$$I_2 = k_2 I_1 \sin^2(k_1 k_3 D^2) \quad (18)$$



(a)



(b)

Fig. 20 - Hysteresis characteristics of PLZT
(a) Linear material (9% La) (b) Storage material (8% La)

These equations do not take into account the variation in charge density over the gap, but nevertheless they give an indication of the shape of the characteristic obtained. It will be seen from Equation (16) that the electro-optic behaviour is quadratic (Kerr effect). Because D is related to the applied voltage by a hysteresis characteristic, a plot of I_2 versus V , the applied voltage, shows a similar relationship to Equation (18), but with hysteresis superimposed. The characteristics of several samples of PLZT material were measured on an oscilloscope and some of the results are shown in Fig. 20. This shows the light output (Y -axis) as a function of the applied voltage (X -axis; centre of screen is zero volts). Fig. 20(a) shows the transfer function of a high-lanthanum (9%) material; there is a moderate amount of hysteresis and the half-wave voltage is approximately 180V. Fig. 20(b) shows the response of a lower-lanthanum (8%) material with the same electrode geometry. The material is much more sensitive but the hysteresis is so great that the trace is very confused and it is not possible to define a unique half-wave voltage; the material also saturates at high fields.

The sensitivity of PLZT reduces as the lanthanum content, or the temperature, is increased. The 9% La material represents a good compromise between low hysteresis and high sensitivity.

4.4. Design of electrodes

Because PLZT has a high dielectric constant, each modulator gap may have a significant capacitance which presents a load on the driving circuits. The way to minimise this capacitance is to reduce the volume of PLZT driven by the applied field, which means small electrode-dimensions and the use of lenses to focus the light beam so that it passes through the small modulator gap. Unfortunately, as the gap between the electrodes is made narrower so the penetration depth of the fringing field in the PLZT is reduced. This effect is shown in Fig. 21, where the calculated field strength in the middle of the gap is plotted as a function of distance below the electroded surface (see

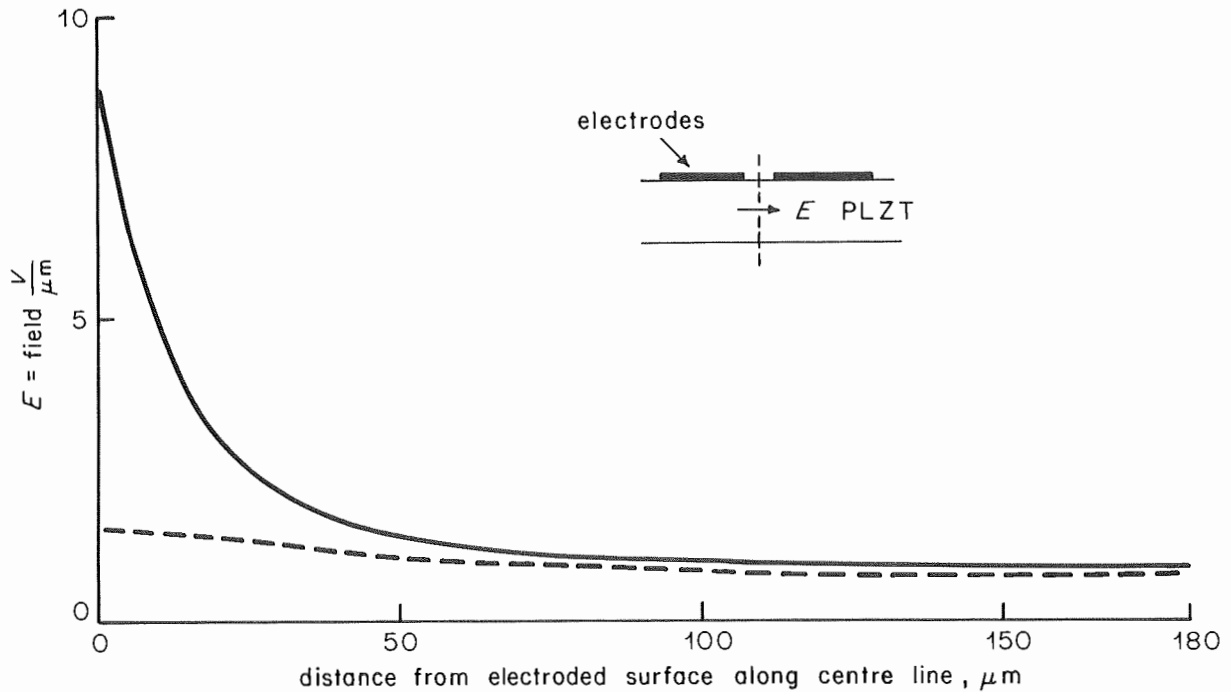


Fig. 21 - Variation of electric field with depth in PLZT slice
 ————— 40 μm gap - - - - - 100 μm gap

inset diagram) for a 40 μm gap and for a 100 μm gap. This can lead to inefficient use of the PLZT slice. Calculations indicate that there is a broad range of optimum gap-dimension centred on one third to one half of the thickness of the PLZT slice. For a slice 180 μm thick, the optimum gap is therefore between 60 μm and 90 μm .

For the smaller gap dimension, further calculations show that the width of the electrodes should be at least twice the gap dimension to ensure maximum field at the centre of the gap for a given applied voltage. This may be

seen from Fig. 22, which shows the relative field strength at the gap centre (near to the electroded surface) as a function of the distance from the gap centre.

Measurements taken for different modulator-electrode dimensions tend to confirm the calculations for half-wave voltage. In particular it is found that increasing the ratio of the electrode width to the spacing (gap) from 1:1 to 2:1 decreases the half-wave voltage by about 15%. Further increases only reduce the half-wave voltage by a maximum of 5%.

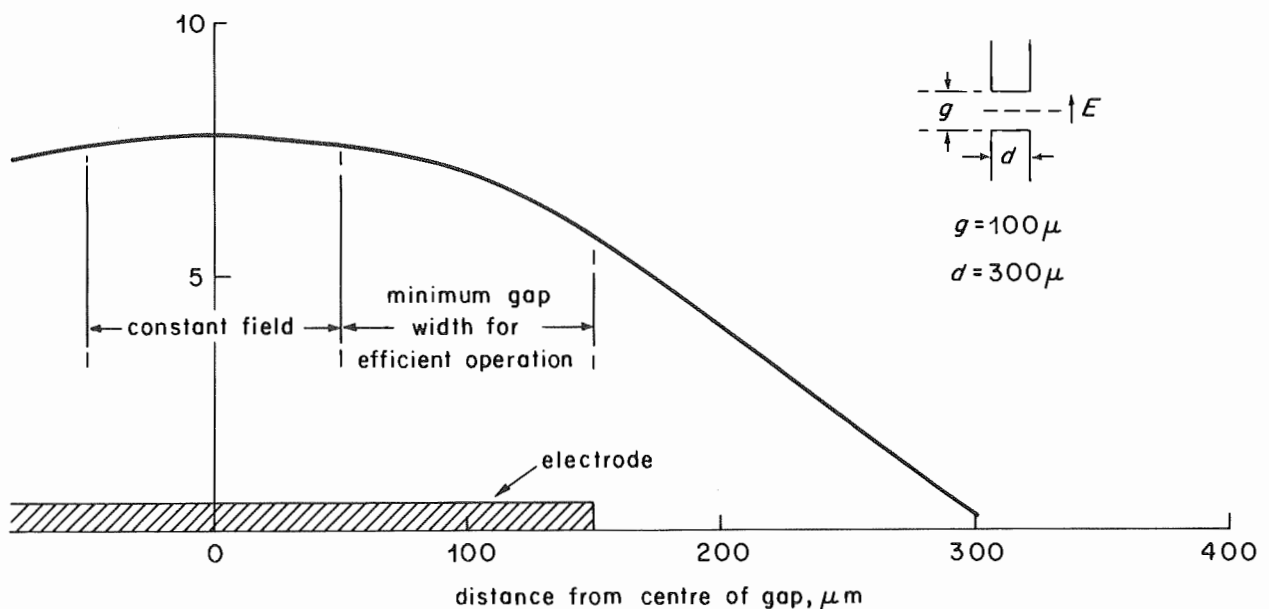


Fig. 22 - Variation of field along the surface of the PLZT modulator

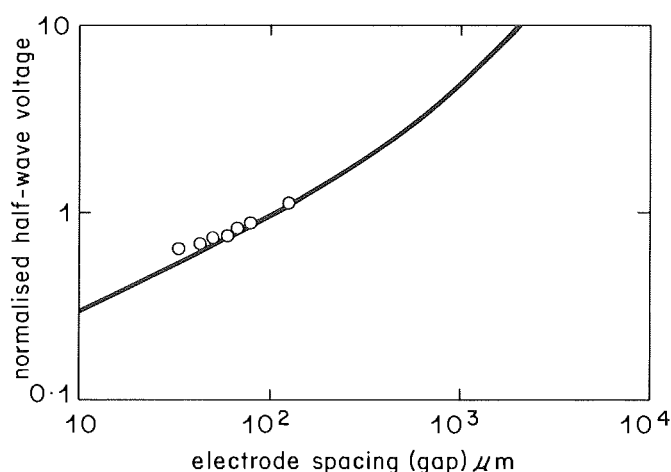


Fig. 23 - Normalised half-wave voltage as a function of electrode spacing (i.e. gap) for a 180 μm thick slice of PLZT

The effect of increasing the electrode spacing is shown in Fig. 23, where the relative half-wave voltage is plotted as a function of the gap dimension; the solid curve was calculated and the open plot points are measured values. It is seen that the agreement is fairly close. The values of inter-electrode capacitance for each modulator, however, are four or five times higher than the 7 pF predicted. An explanation of this is given in a later section.

Thus the optimum modulator electrode dimensions for a slice of PLZT 180 μm thick are: spacing 60 μm , width 120 μm . In practice, the corners of the electrodes are rounded thus reducing the area of uniform field inside the PLZT. Because of this, and because of the difficulty of keeping a beam of light centred on the gap, the electrode width used in prototype modulators was increased to 250 μm .

4.5. Switching performance of PLZT

Square waves of different frequencies were used to drive prototype PLZT modulators. The modulator output (i.e. light intensity versus time) for a range of drive frequencies are typically as shown by the oscilloscope traces in Fig. 24; in each picture the upper trace refers to the applied voltage and the lower to the light intensity at the output. It will be noticed, from the overshoot effect on the traces, that there is a change in the sensitivity with time of application of the driving voltage; in fact, this change amounts to an increase in sensitivity and it is not clear why this should be. One possible cause is a field-assisted thermal drift of domain walls after the initial rapid change caused by application of the driving voltage. However, over a reasonable frequency range, the performance is fairly constant. Contrast ratios of 100:1 or more are obtainable with transition times of about 100 ns. Good contrast ratios can be obtained largely because of the excellent 'off' state of the modulator which arises from the absence of natural birefringence combined with the quadratic electro-optic law.

As the driving frequency is increased, a point is reached at which the sensitivity falls off abruptly. This

reduction in sensitivity is probably due to internal heating as the ceramic is cycled around its hysteresis loop. To check this hypothesis, the ceramic was driven with a multi-burst waveform as shown by the series of oscilloscope traces in Fig. 25. By varying the repetition rate of this waveform, the average number of transitions per second could be altered without changing the multiburst spectrum. The results show that short bursts of 1 MHz modulation can be obtained with no loss of sensitivity when the average transition rate is low (low repetition rate of multiburst). Further, there is very little difference in the relative response of the PLZT to the difference component frequencies of the multiburst even when the general level of sensitivity has fallen considerably at the high repetition rate (see the results at 10^6 transitions per second, for example).

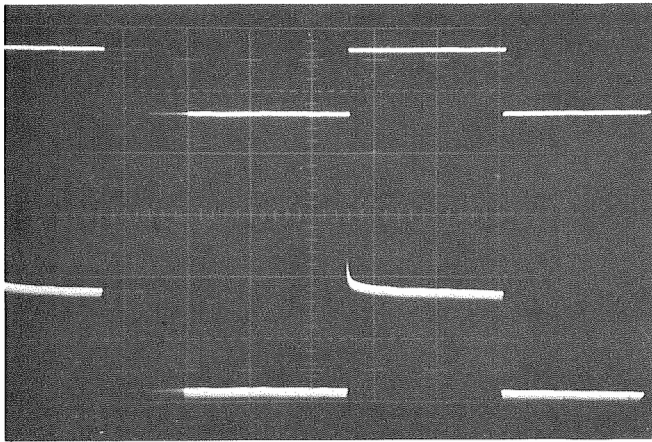
To obtain some idea of the degree of the internal heating, a further experiment was tried. The average transition rate was kept constant (at about 60×10^3 per second) and the temperature of the substrate was then increased by external means. The drop in light output for a temperature increase of 40°C was then measured as only 20%. In order to account for the 50 or 60% drops previously measured at the 10^6 transitions per second rate, it is estimated that the temperature rise in the gap must be of the order of 100°C .

A 2 Megabit per second, NRZ, data stream has 10^6 transitions in level per second, on average.* The 50% drop in light level obtained at this rate is not as serious as it might seem because the no-voltage or 'off' condition is unaffected and the contrast ratio is still very good: therefore, provided the signal-to-noise ratio on replay of the optical recording is adequate, the information can still be recovered.

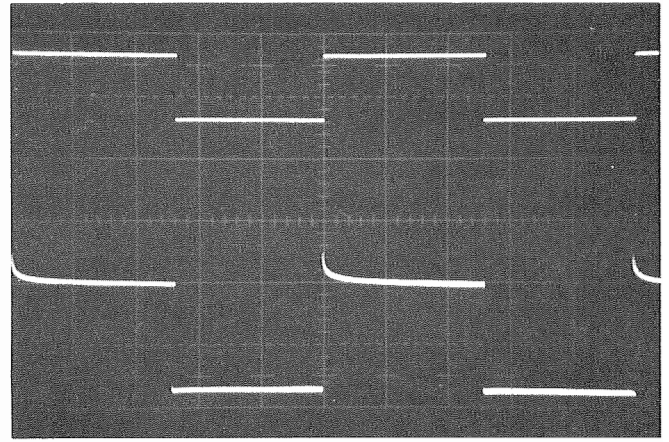
Nevertheless, an investigation was carried out to see if there were operational methods of reducing this fall in sensitivity at high average transition rates. One possible way would be to servo the light level after modulation and control the laser power or modulator drive-voltage to compensate for reduction in modulator efficiency. This method is rather complicated, although it may be worth considering if sensor arrays become sufficiently inexpensive. A better way, perhaps, would be to reduce the degree of heating in the PLZT. The heating is extremely local; mounting the PLZT on a metal backing plate did not reduce it significantly; this is probably because the majority of the temperature gradient occurs in the thickness of the PLZT itself. Reducing the thickness of the PLZT may help, as may further improvement in PLZT compositions or manufacturing techniques.

One method of doubling the frequency range of the PLZT is to reflect back the light by means of a mirror placed close to the far side. The light then passes twice through the gap and the half-wave voltage is reduced to about 71% of its former value (the birefringence is quadratic

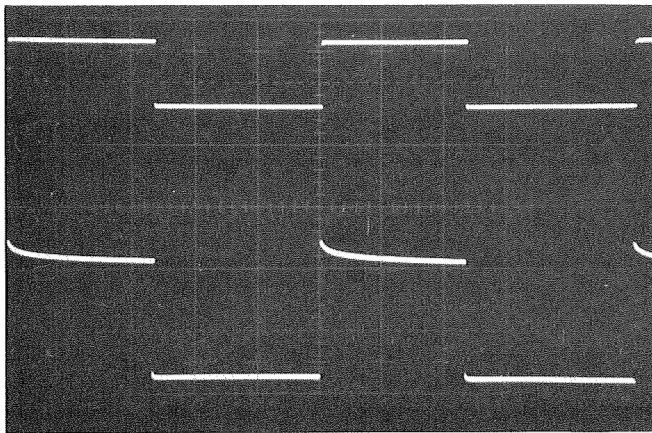
* This assumes a probability of 50% that successive bits are of opposite sign such as would be obtained with a random noise signal input. Work by C.K.P. Clarke of this Department has shown that, for a television signal, the probability is usually lower than this.



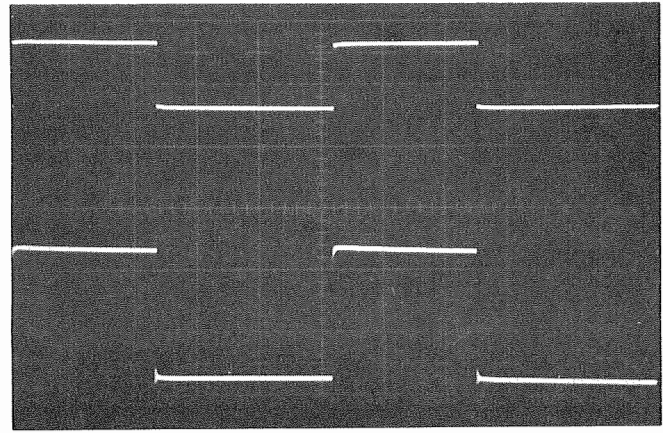
(a)



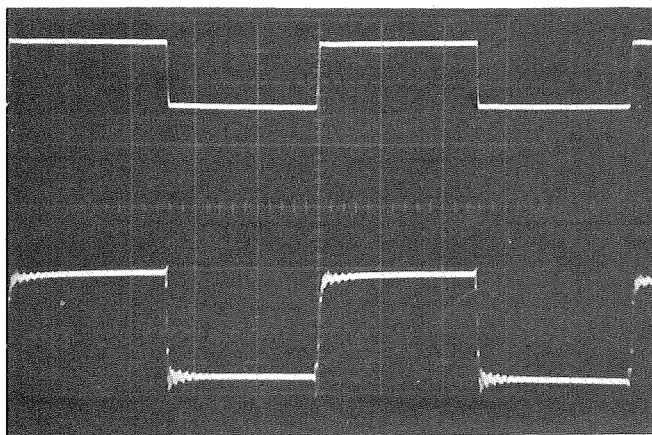
(b)



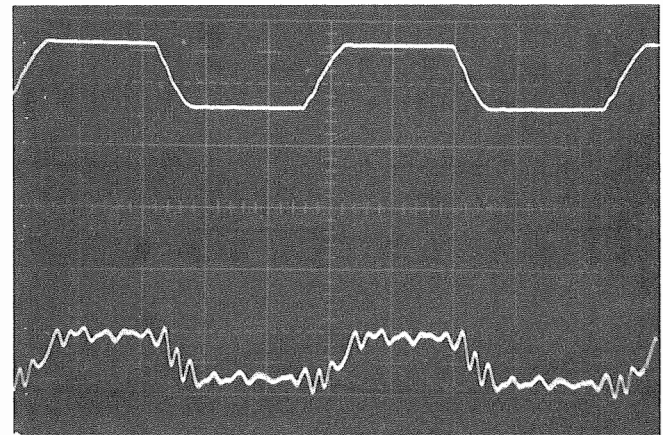
(c)



(d)

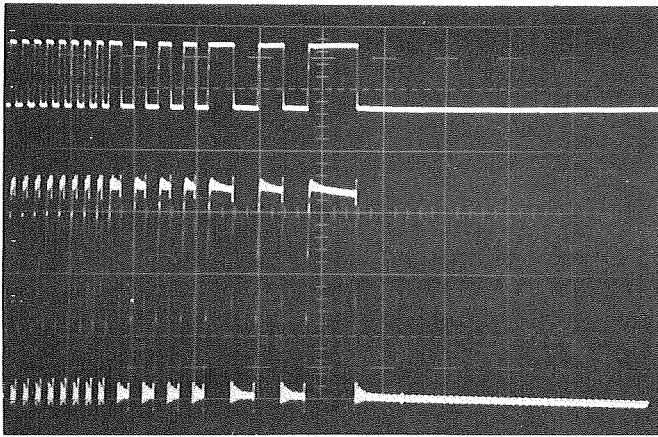


(e)

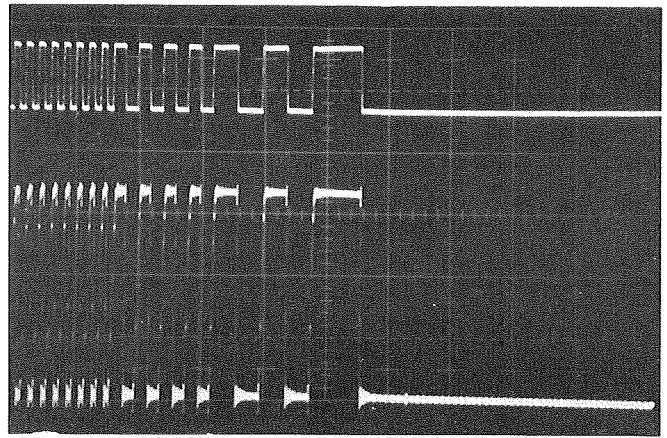


(f)

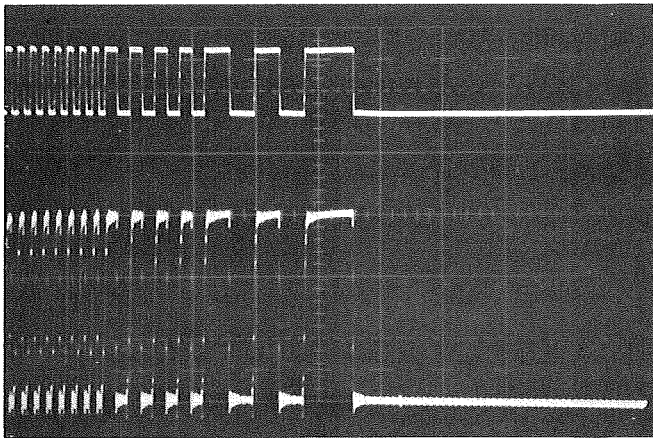
Fig. 24 - Response of PLZT modulator to square-waves of various fundamental frequencies, as indicated
 (a) 10 Hz (b) 100 Hz (c) 1 kHz (d) 10 kHz (e) 100 kHz (f) 1 MHz



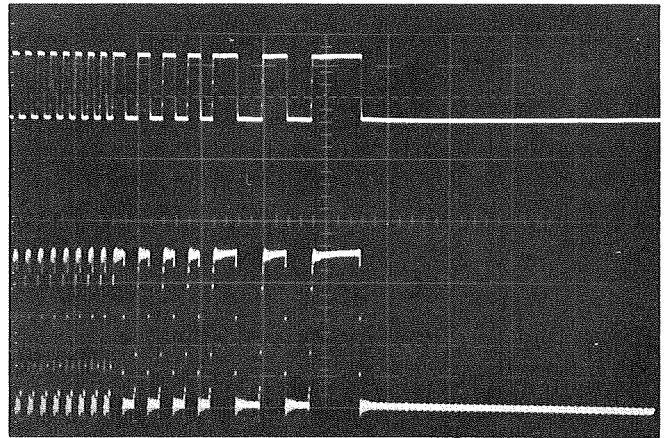
(a)



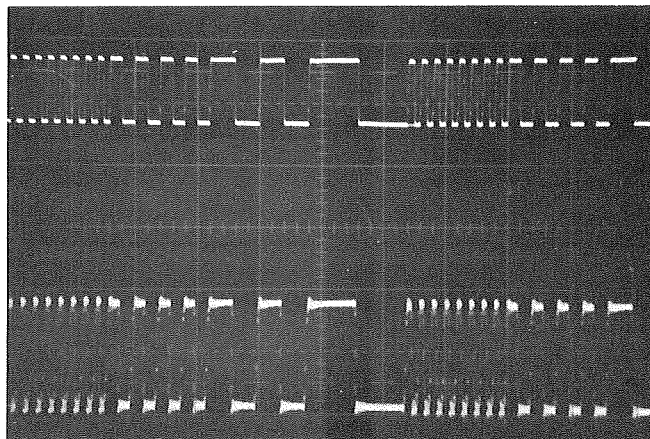
(b)



(c)



(d)



(e)

Fig. 25 - Response of PLZT modulator to a multiburst waveform with various repetition rates
 (a) 64×10^3 transitions per second (b) 125×10^3 transitions per second (c) 250×10^3 transitions per second
 (d) 500×10^3 transitions per second (e) 10^6 transitions per second

with applied field). The heating is thus halved and the frequency range effectively doubled. The drop in sensitivity at the 10^6 transitions per second rate would be reduced to only 10–20% using this reflection mode.

The heating effect is marginally less for smaller electrode spacings than that deduced in the previous section. This is perhaps because of the smaller volume of PLZT heated; the ratio of surface area to volume increases with decreasing size, thus making heat losses proportionately greater but this is offset by the greater field strengths inside the smaller volume.

Some authors have reported fatigue failures of PLZT. Tests we have carried out on a prototype modulator showed that after more than 4×10^{11} switching operations the characteristics were unaltered. This could be because the size of the modulator is so small that any piezo-electric effects can be absorbed by the surrounding volume.

Due to the high refractive index of PLZT, light cannot pass through a thin slice at an angle (to the normal) of greater than about 25° . Thus there is very little variation in half-wave voltage as the angle of incidence is changed; tests on prototype devices showed that, if there was any such variation, it was below the level of the small variations normally found between one area and another on the slice (approximately 10%).

One unwanted characteristic of PLZT is a slight photoconductivity. This is not so severe as to load the driving circuits but produces the situation illustrated in Fig. 26, which shows the equivalent circuit of an illuminated modulator gap. The illuminated portion of the gap has a higher conductivity than the rest.

The effect on the modulator output is shown in Fig. 27, where a switching waveform with high mean voltage is

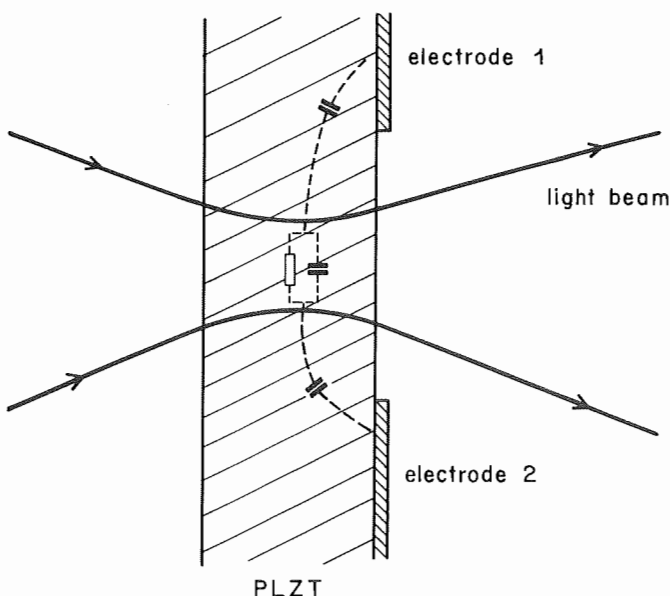
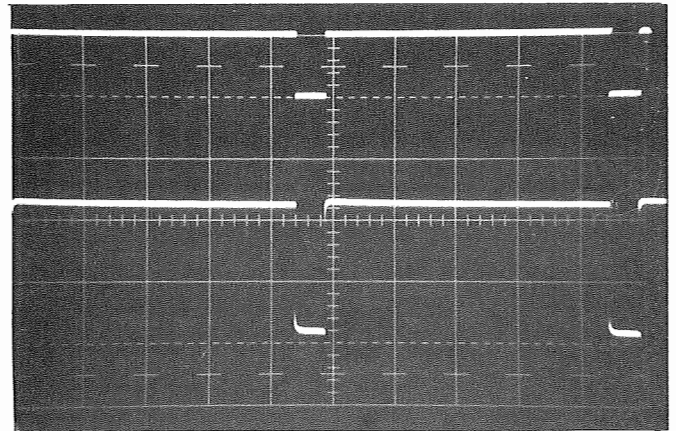
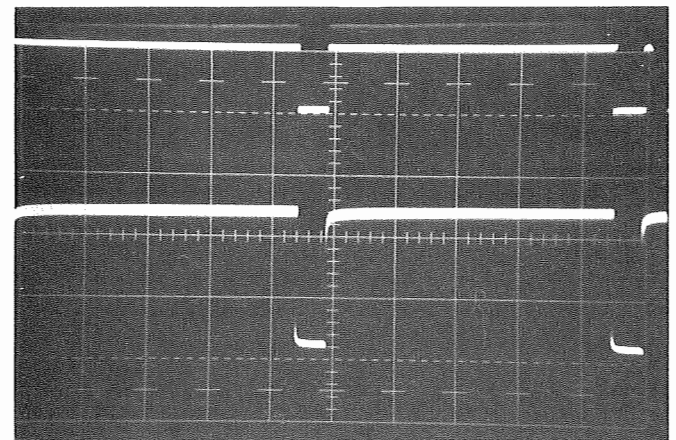


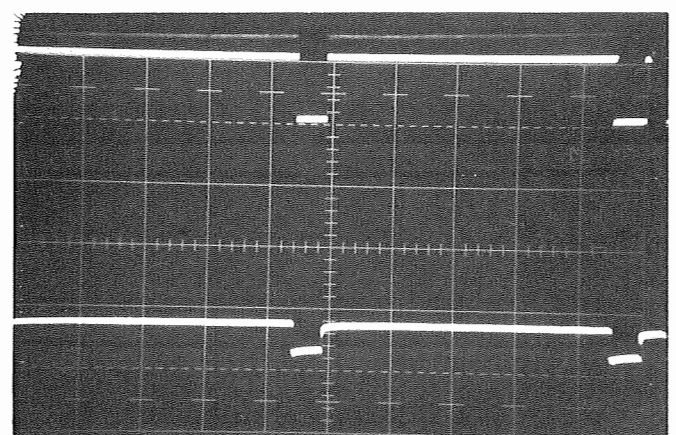
Fig. 26 - Mechanism of photoconductive degradation of PLZT modulator performance



(a)



(b)



(c)

Fig. 27 - Effect of photoconductivity in PLZT: the modulator response to a waveform with a high direct-current component

(a) at initial switch-on

(b) after 5 minutes operation without light passing through the gap

(c) after 5 minutes operation with light passing through the gap

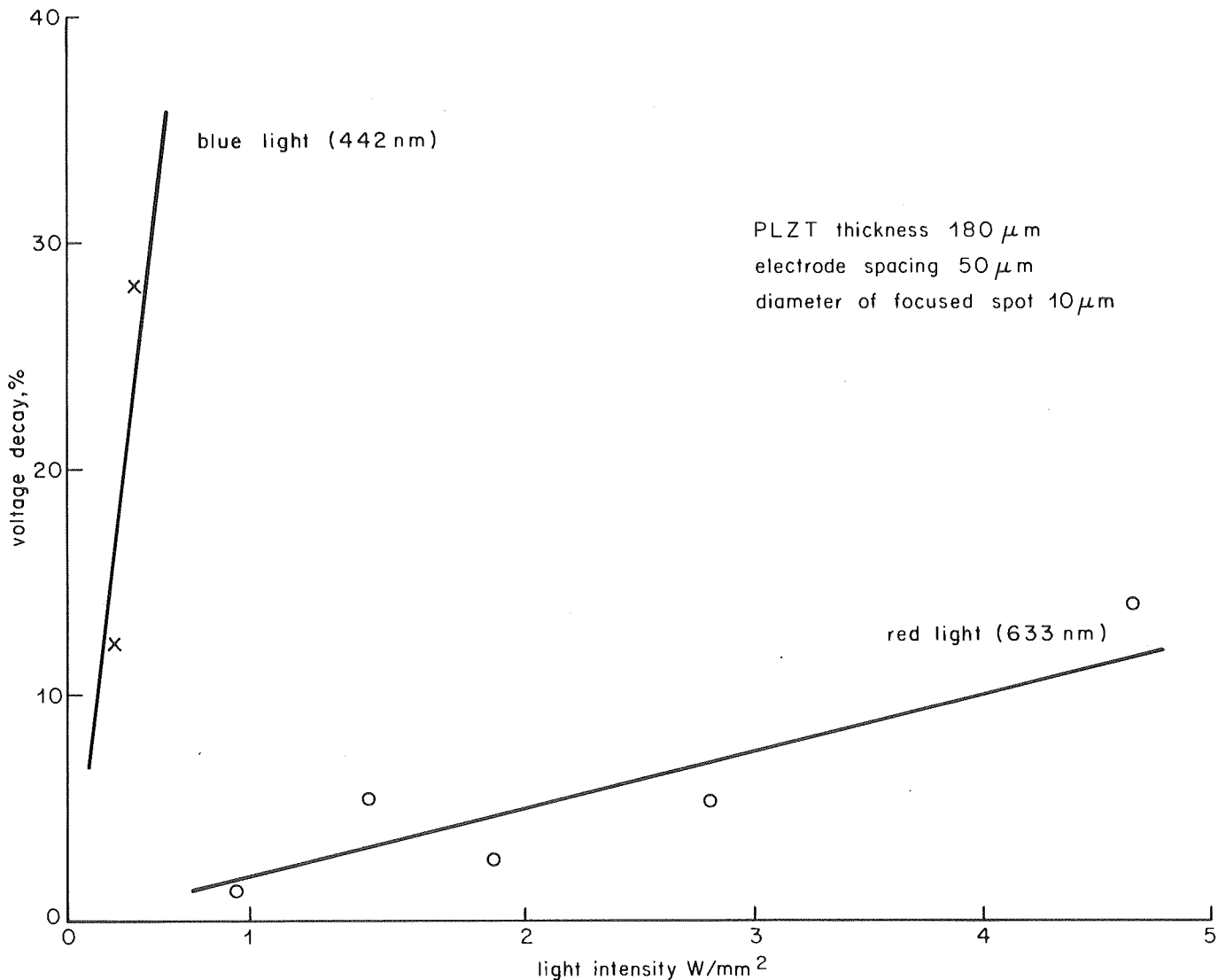


Fig. 28 - Measured decay of mean voltage in PLZT due to photoconductivity, as a function of light intensity in the gap, for two optical wavelengths. (Duration of measurement = 5 minutes)

—X—X— Blue light ($\lambda = 442 \text{ nm}$) —O—O— Red light ($\lambda = 633 \text{ nm}$)

applied. The traces in Fig. 27(a) and 27(b) show that, without light passing through the gap, for any significant period, the modulator response is unchanged. Fig. 27(c) shows that, with light passing through the gap for some 5 mins, the average level of the field across the illuminated region of the PLZT has decreased, giving rise to a corresponding decay in contrast. This decay has been measured as a function of light power for different optical wavelengths. The results are shown in Fig. 28 where the effect is seen to be much greater with blue light.

There are several solutions to this problem. One is the use of bias lighting to swamp the effect of the laser beam but, unfortunately, this requires very high levels of bias lighting. Another is to defocus the laser beam so that it covers the whole gap; this lengthens the time constant considerably (by a factor of at least 20 for a spot diameter of $4/3$ the gap width) but also decreases the transmitted light. This is the simplest method and is suitable for applications where the optical efficiency of the modulator is not required to be very high.

The best solution is to drive the PLZT with a waveform of effectively zero average d.c. content. This can be achieved by using a three-level driving waveform as shown in Fig. 29(a). Alternatively, the 'earth' electrode potential

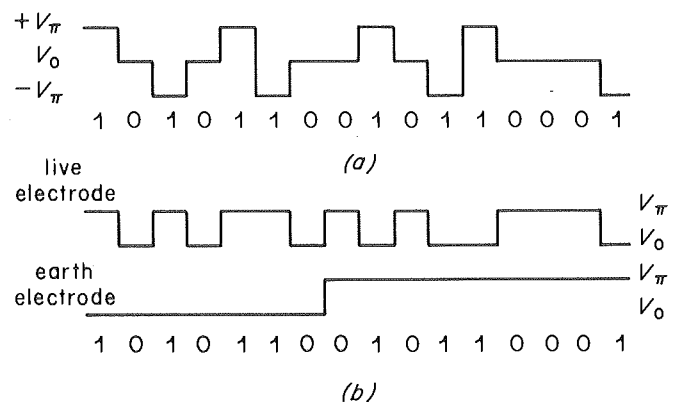


Fig. 29 - Possible coding methods to reduce the effect of photoconductivity

can be periodically alternated between true earth and the half-wave voltage as in Fig. 29(b). In the case of a digital television signal, this switching could be carried out during field blanking or even line blanking if the photoconductive effect is very large. The recorded signal, and hence the replay arrangements, would be unaffected.

4.6. Multiport configurations

Hitherto, only one modulator port has been considered. When there are several ports on a single slice of PLZT more problems arise. The first of these is finding a good method of focusing many beams onto a registered pattern of electrodes. This can be done by using a 'hololens'; consisting of a hologram of the desired pattern of focused spots. When a coherent light beam is passed through the hololens it can be made to form a real image of the desired pattern. If the hololens is a thick phase hologram, optical efficiencies can theoretically be 100%. Unfortunately, very high efficiencies are difficult to realise in practice.

Alternatively an array of phase zone-plates can be used. Experimental phase zone-plates, made using photoresist and a linear developer, yielded optical efficiencies of about 30%.

Another possibility is to assemble an array of small lenslets. Moulded acrylic lenses, for example, are relatively inexpensive and they can be ground square for more efficient packing. With this solution the principal difficulty is registering the optical axes of the lenslets with the corresponding electrode gaps.

Another problem, when there are many modulators on

a single slice, is crosstalk between adjacent modulator gaps due to the high dielectric-constant of the PLZT. One solution is to keep the lead-in conductors short and well separated, and another is to shield them from each other by means of earthed conductors. Where this is not possible, however, or where it would lead to large stray capacitances it is possible to use a more sophisticated technique; this is to run the lead-in connectors to the gaps over a 25 μm thick dielectric layer (of low dielectric constant) applied to the PLZT surface by conventional screen printing. The dielectric is laid down such that it contains a pattern of holes, as illustrated in Fig. 30, which refers to an experimental 8-port design. Because of the limited resolution of the screen printing process, and the viscosity of the ink, the sides of the holes are gently sloping. The conductors run down the sides of the insulating layer and make electrical contact with the modulator electrodes, which are within the holes in intimate contact with the PLZT.

Because the lead-in connections are on the dielectric, which has a low relative permittivity, they are well isolated from each other. This reduces the crosstalk from adjacent interconnections considerably. The crosstalk in an experimental 8-port modulator (see Fig. 30) was measured by driving seven of the ports with the same waveform (of peak value equal to the half-wave voltage) and measuring the light modulation by the remaining port with its driving circuit disconnected. The crosstalk was below the electrical noise level and therefore difficult to measure precisely but was estimated to be -30 dB to -40 dB with reference to the signal level obtained when the port was driven. For comparison, the corresponding figure for an earlier modulator having no dielectric overlay was only -10 dB . This was in spite of a reduced lead-in connection length (the lead-in connections were only 20% of the length used in the 8-port

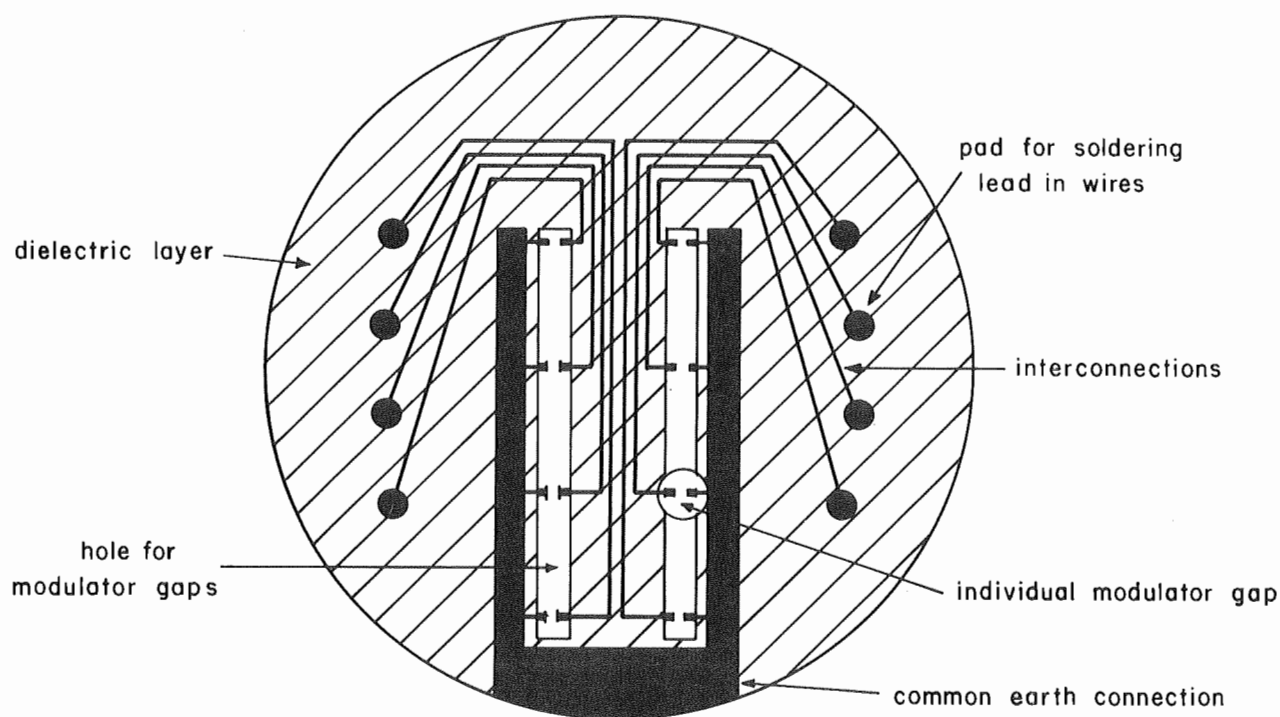


Fig. 30 - Construction of an eight-port modulator using dielectric insulation for the lead-in connectors to reduce crosstalk

design) and a reduced number of driven ports (only one port driven instead of seven).

A beneficial side-effect of this fabrication technique is the reduction of the load capacitance per modulator port. Originally, a major part of this capacitance was, in fact, due to the interconnections; isolating these reduced the capacitance from 35 pF to 22 pF (average). Further reduction might result from decreasing the size of the holes in the dielectric to the point at which the field in the gap begins to be affected. Thus the theoretical results of Section 4.4 may be a realistic estimate of what can eventually be achieved.

The electrodes themselves must be capable of withstanding considerable stress, (pulses of about 500 mA are present when the gap is being switched). Thin evaporated aluminium electrodes were tried but these eroded quickly with use (after approximately 1/2 hr. at the maximum switching rate the electrodes were useless).

A superior method was developed in which the whole of the PLZT was first coated with a thin layer of aluminium bronze. This was then coated with photo resist and the gap electrode pattern formed by exposure through a mask and subsequent development. The exposed areas were then electro-plated to the required thickness with copper. When the resist is removed the substrate is dipped into a suitable etch (mixtures of HCl and FeCl_3 have been used with fair success) which removes the thin film of bronze where it is not covered by the copper. This leaves a relatively thick (5 μm) electrode structure which can be soldered to easily if required.

4.7. Suitability of PLZT for use in a holographic recorder

PLZT meets all the requirements for a page composer for a holographic recording system using up to 100 bits per page. The basic material is relatively inexpensive, sensitive and of reasonable optical quality. The frequency range is just sufficient to record a 2 Megabits per second data stream per modulator port in the straight-through mode but with reduced optical efficiency. With a reflection-mode modulator, the optical efficiency is substantially restored, for this data rate.

The driving circuits are simple; a typical circuit is shown in Fig. 31. This circuit has a low power dissipation especially when the load capacitance is reduced by isolating the lead-in connections. The one troublesome defect, that of photoconductivity, can be overcome with a simple change of driving circuit to eliminate the long term direct-current components of the voltage waveform. A page composer, having a two-dimensional array of 100-ports, can be accommodated with negligible crosstalk on a 50 mm diameter slice of PLZT, complete with lead-in connectors.

5. Conclusions

The various trade-offs between the system parameters are outlined in Section 2. A suggested recording arrange-

ment, for an initial study, involves a line-by-line format of 50-bit holograms and single-axis deflectors with resolutions of at least 120 spots for both the replay and recording processes.

For the recording process, a digital light-deflector seems to be the most promising solution for systems with recording apertures less than $f/2.8$. It is concluded that a seven-stage digital light-deflector comprising KD*P polarisation switches and Wollaston prisms would be feasible for maximum writing rates up to 2 holograms per microsecond with a total beam deflection of 8 degrees. This permits a line of 128 holograms (each subtending $1/16$ degree at the focusing lens) to be recorded in 64 microseconds. The transitional time between spots is limited, at present, to about 200 nanoseconds by the high-voltage circuits driving the polarisation switches. Thus, at the maximum writing rate, the actual 'dwell' time is about 60% of the available exposure time. This aspect could improve significantly if better transistors become available for the high-voltage switches.

In the reading or replay mode, where a continuous motion of the interrogating spot is acceptable, an acousto-optic deflector is recommended and fully-engineered forms are, in fact, available commercially. An additional acousto-optic deflector may prove to be useful for automatic track registration.

In terms of a modest number (several tens) of bits per hologram page, there are a number of feasible solutions including a stack of discrete, low-voltage crystal modulators (e.g. KDP). As the number of bits per hologram page increases (greater than 50, say), methods using a photo-fabricated array of modulator ports on a single slice of electro-optic ceramic becomes more attractive (and certainly less expensive). PLZT ceramic operated in the slim-loop condition (9% lanthanum) is a suitable material for channels working at a data-rate up to two Megabits per second. Switching times of 100 nanoseconds and on/off contrast ratios of 100:1 are typical. Although there are difficulties associated with hysteresis, photoconductivity and heat transfer these can be overcome with proper design and operation. No evidence of material fatigue has been observed in experimental PLZT switches. A disadvantage of this approach is that the incident light has to be focused into the individual modulator ports if good optical efficiency is to be achieved in the device. This requires a corresponding array of external optical components which need very precise registration and alignment.

Further developments of both page composers and deflectors will depend on the assessment of the results of actual writing experiments using partly engineered versions of these devices in an experimental recorder. Most of the future effort relating to modulators and deflectors is expected to be concerned with methods of improving their optical efficiency.

6. References

1. CHEN, D.I. and ZOOK, J. David. An overview of optical storage technology. *Proc. IEEE*, 1975, **63**, 8, pp. 1207 — 1229.

2. LUNN, J.D. and MOFFAT, M.E.B. Possible techniques for the recording of digital television signals. BBC Research Department Report No. 1969/42.
3. TAYLOR, E.W. Recording using hologram arrays: a general survey. BBC Research Department Report No. 1973/40.
4. British Patent Specification. Improvements in the recording of digital television signals. No. 7954/71.
5. HACKING, K. Digital recording using hologram arrays: low-frequency micro-holograms on photographic film. BBC Research Department Report No. 1974/1.
6. AAS, H.G. and ERF, R.K. Application of ultrasonic standing waves to the generation of optical beam scanning. *J. Acoust. Soc. Am.*, 1964, **36**, 10, pp. 1906 – 1913.
7. CHEN, F.S., GEUSIL, J.E., KURTZ, S.K., SKINNER, J.G. and WEMPLE, S.H. Light modulation and beam deflection with potassium tantalate – niobate crystals. *J. Appl. Phys.*, 1966, **37**, pp. 383 – 398.
8. FOWLER, V.J. and SCHLAFFER, J. A survey of laser beam deflection techniques. *Proc. IEEE*, 1966, **54**, 10, pp. 1437 – 1444.
9. HOLT, D. Laser beam deflection techniques. *Optics Technology*, Feb. 1970.
10. KORPEL, A., ADLER, R., DESMARES, P. and WATSON, W. A television display using acoustic deflection and modulation of coherent light. *Proc. IEEE*, 1966, **54**, 10, pp. 1429 – 1437.
11. CHILDS, I. Laser beam deflection. BBC Research Department Report No. 1974/31.
12. NELSON, T.J. Digital light deflection. *Bell Syst. Tech. J.*, 1961, **43**, pp. 821 – 845.
13. TABOR, W.J. A high-capacity digital light deflector using Wollaston prisms. *Bell Syst. Tech. J.*, 1967, **46**, pp. 957 – 990.
14. SOREF, R.A. and McMAHON, D.H. Optical design of Wollaston prism digital light deflectors. *App. Opt.*, 1966, **5**, 3, pp. 425 – 434.
15. KRUGER, U., PEPPERL, R. and SCHMIDT, U.J. Electro-optic materials for digital light beam deflectors. *Proc. IEEE*, 1973, **61**, 7, pp. 992 – 1007.
16. BILLINGS, B.H. The electro-optic effect in uniaxial crystals of the type XH_2PO_4 , 1. Theoretical. 11. Experimental. *Journ. of Opt. Soc. Am.*, 1949, **39**, 10, pp. 797 – 808.
17. BILLINGS, B.H. The electro-optic effect in uniaxial crystals of the dihydrogen phosphate (XH_2PO_4), type, IV. Angular field of the electro-optic shutter. *Journ. of Opt. Soc. Am.*, 1952, **42**, 1, pp. 12 – 20.
18. STEPHANY, J.F. Piezo-optic resonances in crystals of the dihydrogen phosphate type. *Journ. Opt. Soc. Am.*, 1965, **55**, 2, pp. 136 – 142.
19. EKSTEIN, H. Free vibrations of anisotropic bodies. *Phys. Rev.*, 1944, **66**, 108.
20. LEE, M.D. 1970. Solid-state driving of electro-optic light deflectors at high frequencies. Proceedings of the Technical Programme, Electro-optics 71, International Conference, Brighton, England, pp. 207 – 218.
21. FOX, A.J. 1975. Electro-optic materials and their applications. *Electronic Equipment News*, No. 1975, pp. 33 – 36.
22. CARL, K. and GEISEN, K. 1973. Dielectric and optical properties of quasi-ferroelectric PLZT ceramic. *Proc. IEEE*, 1973, **61**, 7, pp. 967 – 974.
23. CUTCHEN, J.T., HARRIS, J.O. (Jr.), and LAGUNA, G.R. 1973. Electro-optic devices utilizing quadratic PLZT ceramic elements. Sandia Laboratories Technical Report No. SLA-73-777.
24. LAND, C.E. and THATCHER, P.D. 1969. Ferroelectric ceramic electro-optic materials and devices. *Proc. IEEE*, 1969, **57**, 5, pp. 751 – 768.
25. NORMAN, S.L. and SINGH, M.D. 1975. Spectral sensitivity and linearity of Shipley AZ 1350 – photoresist. *App. Opt.*, 1975, **14**, 4, pp. 818 – 819.

Appendix

Description of 2 kV switch circuit

Referring to Fig. 14 (under Section 3.3.3) a series of charge drive-pulses is applied to the bases of transistors TR1 to TR6 to produce an output of 2 kV; the transistors are turned on by the pulses and remain on, in the interval between pulses, due to charge storage. To switch the output to earth the pulses to TR1 to TR6 are inhibited and pulses are sent to the other output transistors (TR7 to TR12). The resistors and capacitors across the output transistors are used for equalising the static and dynamic loads of each transistor.

The transformers are single turns of thin insulated wire on an FX2249 core; the use of these cores (larger in cross-sectional area than the toroids used by Lee²⁰), reduces saturation effects in the ferrite and decreases pre-driver power dissipation by about an order of magnitude. Interwinding capacitance is 2.5 pF and the windings break down at 5 kV.

Because the load on the output is greatest when the output changes state a modulated charge drive is used. By this means, the first charge drive-pulse of a series is made larger than the rest. Independent adjustment of each pulse amplitude means that the charge storage in each transistor lasts only as long as the interval between pulses (1 μ sec); this in turn makes the efficiency of the circuit as high as possible. In practice the amplitudes are easy to set and remain stable with use.

The matching balanced transformers in the pre-driver circuit (T7 and T8) perform two functions. One is to

match the output impedance of the pre-driver to the input impedance of the output stage; the other is to provide a balanced path, (via the two secondary resistors) for the current flowing in the primary/secondary capacitances of the FX2249 transformers. Failure to allow this balanced path causes all the current, induced by a change of output state across the interwinding capacitance, to flow to the 150V supply via the FX2249 transformers. This is equivalent to a small charge drive-pulse and it is possible to turn on both sets of output transistors, greatly increasing the power dissipation.

The power requirements are dependent on load but with a typical load of 22 pF the current drawn from a 1.6 kV EHT supply was measured as 50 mA at the maximum switching rate of 10^6 transitions per second. The pre-driver current was 30 mA at this switching rate and the current drawn from the ± 15 V and 5V supplies was insignificant.

The large power dissipation in the output transistors at high switching rates (approximately 8W each at maximum) means that forced liquid cooling must be employed for the fastest stages. A circulating oil system was used in the prototype, but alternative techniques may reduce the power dissipation to a level at which forced air cooling is possible. Examples of such techniques are, sharing the load between two sets of KD*P crystals and drivers (which increases the number of optical components but halves the power required from each driver) and tuning the load (which greatly reduces driver power but at the expense of circuit flexibility and output waveform).

